

2012

Raman Spectroscopy Study of Graphene Under High Pressure

Ali Hadjikhani

Florida International University, ahadj001@fiu.edu

Follow this and additional works at: <http://digitalcommons.fiu.edu/etd>

Recommended Citation

Hadjikhani, Ali, "Raman Spectroscopy Study of Graphene Under High Pressure" (2012). *FIU Electronic Theses and Dissertations*. Paper 656.

<http://digitalcommons.fiu.edu/etd/656>

This work is brought to you for free and open access by the University Graduate School at FIU Digital Commons. It has been accepted for inclusion in FIU Electronic Theses and Dissertations by an authorized administrator of FIU Digital Commons. For more information, please contact dcc@fiu.edu.

FLORIDA INTERNATIONAL UNIVERSITY

Miami, Florida

RAMAN SPECTROSCOPY STUDY OF GRAPHENE UNDER HIGH PRESSURE

A thesis submitted in partial fulfillment of

the requirements for the degree of

MASTER OF SCIENCE

in

MATERIALS SCIENCE AND ENGINEERING

by

Ali Hadjikhani

2012

To: Dean Amir Mirmiran
College of Engineering and Computing

This thesis, written by Ali Hadjikhani, and entitled Raman Spectroscopy Study of Graphene Under High Pressure, having been approved in respect to style and intellectual content, is referred to you for judgment.

We have read this thesis and recommend that it be approved.

Kinzy Jones

Surendra Saxena

Wonbong Choi

Jiuhua Chen, Major Professor

Date of Defense: March 28, 2012

The thesis of Ali Hadjikhani is approved.

Dean Amir Mirmiran
College of Engineering and Computing

Dean Lakshmi N. Reddi
University Graduate School

Florida International University, 2012

ABSTRACT OF THE THESIS

RAMAN SPECTROSCOPY STUDY OF GRAPHENE UNDER HIGH PRESSURE

by

Ali Hadjikhani

Florida International University, 2012

Miami, Florida

Professor Jiuhua Chen, Major Professor

Due to its exceptional mechanical and electrical properties, graphene (one layer sheet of carbon atoms) has attracted a lot of attention since its discovery in 2004. The purpose of this research is to compare the Raman spectra of graphene with plasma treated graphene sheets which have been treated by changing the different parameters affecting the plasma treatment like gas flow, power and pressure and treatment time. The graphene we used for our high pressure studies are 4-5 layer CVD deposited graphene samples prepared by our collaborators in Dr. W. B. Choi's group. First we report a Raman spectroscopy study of graphene on copper substrate at high pressures. Diamond anvil cell (DAC) was used to generate pressure. In situ Raman spectra were collected at pressures up to 10 GPa. The results indicate that the G band of graphene shifts with pressure significantly (about 5 cm⁻¹/GPa) whereas the 2D band changes very little. The plasma treated samples were loaded into DAC. Raman spectrum was captured. Parts of the spectrum which were not related to the graphene peak position were eliminated. The background was reduced. Peaks were found and fitted using FITYK software and the shift of each peak compared to its last position was observed when the pressure was increased. Next we studied plasma treated graphene samples treated with different partial

pressure treatments under high pressure and compared them to each other using zirconia anvil cell with the same method.

TABLE OF CONTENTS

CHAPTER	PAGE
1. INTRODUCTION	1
Overview	1
Motivation and Goal	2
Specific Statement of Research Questions/Objectives	3
Hypotheses	4
Scope of this dissertation	5
2. RAMAN SPECTROSCOPY	5
Nature of Rayleigh and Raman Scattering.....	5
Energy Transfer Model	7
About the patterns of Raman spectra	8
3. GRAPHENE	10
Structure	11
Properties	12
Mechanical	12
Electronic	12
Synthesis	13
Characterization	13
Optical observation and microscopy.....	13
AFM/STM.....	14
Raman Spectroscopy.....	14
4. HIGH PRESSURE EQUIPMENT:DIAMOND ANVIL CELL (DAC).....	14
5. EQUIPMENT AND MATERIALS	18
Raman Stage	18
Anvils.....	19
Diamond.....	19
Zirconia.....	20
6. RESULTS AND DISCUSSION	20
Intro	20
Raman spectroscopy of Samples loaded into DAC	21
Raman spectroscopy of Samples loaded into ZAC.....	25
Partial pressure 75	34
Partial pressure 100.....	36
Partial pressure 125	38
Partial pressure 150.....	41
Partial pressure 175.....	44
Future work.....	46

LIST OF REFERENCES	51
--------------------------	----

LIST OF TABLES

TABLE	PAGE
1. TABLE 6-1.....	34
2. TABLE 6-2.....	35
3. TABLE 6-3.....	36
4. TABLE 6-4.....	36
5. TABLE 6-5.....	37
6. TABLE 6-6.....	37
7. TABLE 6-7.....	38
8. TABLE 6-8.....	39
9. TABLE 6-9.....	40
10. TABLE 6-10.....	40
11. TABLE 6-11.....	41
12. TABLE 6-12.....	41
13. TABLE 6-13.....	42
14. TABLE 6-14.....	42
15. TABLE 6-15.....	43
16. TABLE 6-16.....	44
17. TABLE 6-17.....	44
18. TABLE 6-18.....	45
19. TABLE 6-19.....	45
20. TABLE 6-20.....	45

TABLE OF FIGURES

FIGURE	PAGE
1. FIGURE 2-1	8
2. FIGURE 2-2	9
3. FIGURE 3-1	11
4. FIGURE 4-1	15
5. FIGURE 4-2	16
6. FIGURE 4-3	16
7. FIGURE 4-4	16
8. FIGURE 4-5	17
9. FIGURE 4-6	17
10. FIGURE 5-1	19
11. FIGURE 6-1	21
12. FIGURE 6-2	22
13. FIGURE 6-3	22
14. FIGURE 6-4	23
15. FIGURE 6-5	24
16. FIGURE 6-6	25
17. FIGURE 6-7	27
18. FIGURE 6-8	27
19. FIGURE 6-9	28
20. FIGURE 6-10	32
21. FIGURE 6-11	33

22. FIGURE 6-12	35
23. FIGURE 6-13	35
24. FIGURE 6-14	37
25. FIGURE 6-15	38
26. FIGURE 6-16	39
27. FIGURE 6-17	40
28. FIGURE 6-18	42
29. FIGURE 6-19	43
30. FIGURE 6-20	43
31. FIGURE 6-21	44
32. FIGURE 6-22	45
33. FIGURE 6-23	46
34. FIGURE 6-24	466
35. FIGURE 6-25	47
36. FIGURE 6-26	49
37. FIGURE 6-27	49

1. Introduction

1.1. Overview

Graphene, one layer sheet of carbon atoms, has attracted attention since its discovery in 2004. It is the thinnest yet the strongest material ever measured. In addition, charge carriers in graphene can sustain currents six order of magnitude higher than copper. Together with many other superior thermal conductivity and elastic stiffness, properties of graphene make this material extremely attractive to material scientists, physicists and electronic engineers. In general the current attention to graphene could be attributed to three main reasons: First, it has unique electron transport phenomena, which allows for the investigation of relativistic quantum phenomena in a bench top experiment. This reason is out of the scope of this research and will not be discussed further. Second, graphene is a promising candidate for nano applications. Its ballistic transport, mechanical and chemical stability at room temperature extend to the bilayer and few layer graphene and therefore make it a suitable material for nano applications. Third, graphene is the building block for nearly all carbon allotropes. It has been studied theoretically for over 60 years and all forms of Graphite, nano tubes, etc can be considered as its derivatives. Monolayer graphene can be obtained by micromechanical cleavage. Other procedures such as exfoliation and growth yield multi layer graphene. Unit cell of monolayer graphene has two carbon atoms, A and B, each of which forms a triangular 2D network, and they are linked by the carbon-carbon bonds with $a_{C-C}=0.142$ nm. On the other hand, graphite is a bernal stacking of monolayer graphene in which carbon atoms on the corner locate above the vacant sites of a hexagon on another layer.

Graphite unit cell has four carbon atoms on the two layer planes and has Lattice constants $a=0.246$ nm and $c= 0.670$ nm.^[3]

1.2. Motivation and Goal

To date, except for Proctor et al. (2009), there are no studies published on graphene at high pressures and this is surprising considering the growing interest in the mechanical properties of graphene and its possible application in nano electronics. Taking into account the predicted dependence of electronic band gap on strain, it is very important to apply strain and monitor strain. Since Raman spectrum allows unambiguous, high-throughput, nondestructive identification of graphene layers^[5], study of graphene at high pressure combined with Raman spectroscopy has the potential to develop into an important component in the characterization and understanding of this remarkable new material. Also it has been shown that the electronic structure of graphene indicated by its Raman spectrum clearly evolves with the number of layers. The D peak changes in width, shape and position as the number of layers increase, whereas the G peak shows a slight red shift. When the number of atomic layers increases above 5, the Raman spectrum becomes hardly distinguishable from that of the bulk graphite.^[3] Yet graphene has one major problem which makes its use in optoelectronics and electronics particularly difficult. Monolayer graphene is a gapless semi-metal. For some of the applications, especially in switching and logic, a band gap is required. There are a number of solutions to approach this problem. One way is to functionalize its basal plane with foreign atoms. With proper functionalization a finite band gap can be opened at its charge neutrality level; this will introduce graphene as a building block for electronics applications where a resilient on/off switch is always on demand. In the Raman spectrum of graphene, the D

peak is a measure of defects or a measure of breaking of the planar sp^2 symmetry in the graphene lattice such as the graphene edges. Consequently the I_D/I_G ratio yields a measure of the ratio of the non- sp^2 to sp^2 bonding character in a carbon-based material.^[4] One of the motivations of this thesis was to improve the pre-existing methods to characterize graphene and to better understand graphene's electronic band structure through Raman spectroscopy of CVD grown few layer graphene under hydrostatic pressure. Another goal of this research is to functionalize CVD grown graphene using plasma treatment to open a finite band gap and then study the relation between different parameters of plasma treatment and band gap opening. Another aim would be to monitor how band gap opening is affected with applying pressure in each of the plasma treatment levels. Band gap opening could be studied if the electronic band structure can be captured. That is where Raman spectroscopy plays a key role. A relation between the band gap opening and the plasma treatment would enable further research on controlling the band gap width, which as mentioned above will eventually introduce graphene as a building block for electronics applications where having an on/off switch is of critical importance.

1.3. Specific Statement of Research Questions/Objectives

The purpose of this research is to compare the Raman spectra of graphene samples before and after plasma treatment. Effect of different plasma treatment parameters is also investigated. The graphene we used for our high pressure studies are 4-5 layer CVD deposited graphene samples prepared by our collaborators in Dr. W. B. Choi's group. Some of the TEM images in this thesis are taken from the samples we received from (RPI) Dr. Koratkar's group and they are graphene platelets and plasma treated graphene

platelets. First we report a Raman spectroscopy study of graphene on copper substrate at high pressures. Diamond anvil cell (DAC) was used to generate pressure. In situ Raman spectra were collected at pressures up to 10 GPa. The result indicates that the G band of graphene shifts with pressure significantly (about 5 cm⁻¹/GPa) whereas the 2D band changes very little. The change of the peak when we have plasma treatment will be discussed. Then the plasma treated samples were loaded into DAC. Raman spectrum was captured. Parts of the spectrum which were not related to the graphene peak positions were eliminated. The background was reduced. Peaks were found and fitted using FITYK software and the shift of each peak compared to its last position was observed when the pressure was increased. Next we studied plasma treated graphene samples treated with different partial pressure treatments under high pressure and compared them to each other using zirconia anvil cell with the same method.

1.4. Hypotheses

Raman G peak position is predicted to show an upshift by increasing the pressure. The same trend is expected for the G' peak according to Proctor et al. (2009).

Proctor et al. (2009) have studied Raman spectroscopy of graphene under hydrostatic pressure. The samples that they used for their study were monolayer, bilayer and few layer graphene supported on silicon, along with unsupported graphene samples. The samples our group and our collaborators used were CVD grown 4-5 layer graphene on copper. The results Proctor et al. achieved will be used as a guideline but since the samples are not exactly the same we cannot investigate the accuracy of our results by referring to the aforementioned article. However, comparisons to the article will be presented in different parts of this text.

1.5. Scope of this dissertation

A brief introduction about the motivation, goals and objectives of this research is given in this first chapter. The second chapter of this thesis presents some background and literature review in which the Raman Spectroscopy and different methods of Raman Spectroscopy will be discussed. The third chapter of this thesis is dedicated to an introduction of graphene, methods of its synthesis and characterization methods. The fourth chapter discusses the high pressure equipment (DAC) and anvils commonly used for reaching high pressures. The fifth chapter discusses the equipment and materials used in this thesis, including descriptions of their advantages and disadvantages. In chapter six the primary results of this research are presented. Problems and difficulties encountered during the research are also discussed and necessary future work to improve the results is suggested.

2. Raman Spectroscopy

Raman Spectroscopy is a characterization process which uses scattered light to identify materials. It won Professor C.V Raman the Physics Nobel Prize in 1930.

2.1. Nature of Rayleigh and Raman Scattering

When we have monochromatic radiation on systems such as dust-free, transparent gases and liquids, or optically perfect, transparent solids some scattering of radiation happens. If the scattered radiation is to be analyzed it will be observed not only the incident wave number but also pairs of new wave numbers of the form $\nu = \nu_0 \mp \nu_m$. In molecular systems, ν_m lies in range of the transitions between rotational, vibrational, and electronic levels. The scattered radiation usually has different polarizations as compared to incident beam and intensity and polarization changes depending on the direction of the

observation. Scattering of radiation with change of frequency is called Raman scattering. It was first observed in the liquids in 1928 by C.V. Raman. In the spectrum of the scattered radiation new wavenumbers are called Raman lines or bands and collectively make a Raman spectrum. Raman bands which possess wavenumbers that are less than incident wavenumber are called Stokes band. The ones greater than the incident wavenumber are called anti-stokes bands. Scattering can also happen because of the Doppler effect which is called Brillouin and is usually very small (order of 0.1 cm^{-1}) so it cannot be separated from the scattered radiation for Raman studies. Scattering of radiation without the change of frequency was known before the discovery of the Raman and it was called the Rayleigh scattering after Lord Rayleigh. It will always accompany Raman scattering unless selective filters are employed. Rayleigh scattering accompanying Raman actually has its own advantages. It can serve as a reference for determination of ν_m . Scattering of radiation without change of radiation, referred to as Mie scattering, happens because of larger scattering centers like dust particles. This kind of scattering can be very intense and it would be usually present unless extraordinary efforts are made to remove the dust particles and other Mie scatterers from the system. As a result, what is usually referred to as Rayleigh scattering, consists of true Rayleigh scattering, together with some Mie and unresolved Brillouin scattering. It is relatively difficult to make a generalization about the relative intensities since they depend on many factors. However, usually the intensity of Rayleigh scattering is about 10^{-3} of the intensity of the incident radiation. And the intensity of strong Raman bands is usually 10^{-3} of the intensity of Rayleigh scattering.

2.2. Energy Transfer Model

The origin of the change of the wavenumbers in Raman scattering may be explained in terms of energy transfer between the system and the beam. When a system interacts with the incident beam it might shift to an upper energy level of E_2 from a lower E_1 energy level. For this to happen, the system should acquire the $\Delta E = E_2 - E_1$ from the incident beam. The energy might be expressed in terms of the wavenumbers associated with the involved levels. This can be regarded as annihilation of one incident photon and simultaneous production of a lower energy photon. Also, the aforementioned radiation may cause a downward transition from a higher energy to a lower energy level. This occurs only if the system is already in the excited level and has a lower probability. In the case of Rayleigh scattering the incident photon annihilates but a photon of the same energy gets created simultaneously.

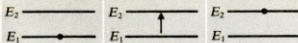
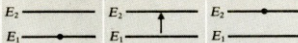
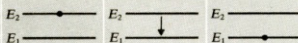
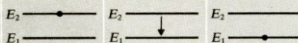
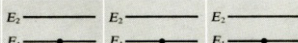
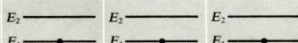
		Initial state	Process	Final state
(a) Stokes Raman scattering	Radiation	$hc\tilde{\nu}_0$	Annihilate $hc\tilde{\nu}_0$ Create $hc(\tilde{\nu}_0 - \tilde{\nu}_{M})$	$hc(\tilde{\nu}_0 - \tilde{\nu}_{M})$
	Scattering system			
	Total energy	$hc\tilde{\nu}_0 + E_1$		$hc(\tilde{\nu}_0 - \tilde{\nu}_{M}) + E_2$
(b) Anti-Stokes Raman scattering	Radiation	$hc\tilde{\nu}_0$	Annihilate $hc\tilde{\nu}_0$ Create $hc(\tilde{\nu}_0 + \tilde{\nu}_{M})$	$hc(\tilde{\nu}_0 + \tilde{\nu}_{M})$
	Scattering system			
	Total energy	$hc\tilde{\nu}_0 + E_2$		$hc(\tilde{\nu}_0 + \tilde{\nu}_{M}) + E_1$
(c) Rayleigh scattering	Radiation	$hc\tilde{\nu}_0$	Annihilate $hc\tilde{\nu}_0$ Create $hc\tilde{\nu}_0$	$hc\tilde{\nu}_0$
	Scattering system			
	Total energy	$hc\tilde{\nu}_0 + E_1$		$hc\tilde{\nu}_0 + E_1$

Figure 2-1

Representation of (a) Stokes Raman scattering, (b) anti-Stokes Raman scattering, and (c) Rayleigh scattering. Adapted from [7]

2.3. About the patterns of Raman spectra

The form of Raman spectra that is being observed depends on the energy level in the scattering system, the permitted transitions, and the observation conditions, power of the analyzing instrument in particular. The energy levels of molecular systems fall into particular patterns so for each of these systems a specific form of Raman spectrum can be expected.

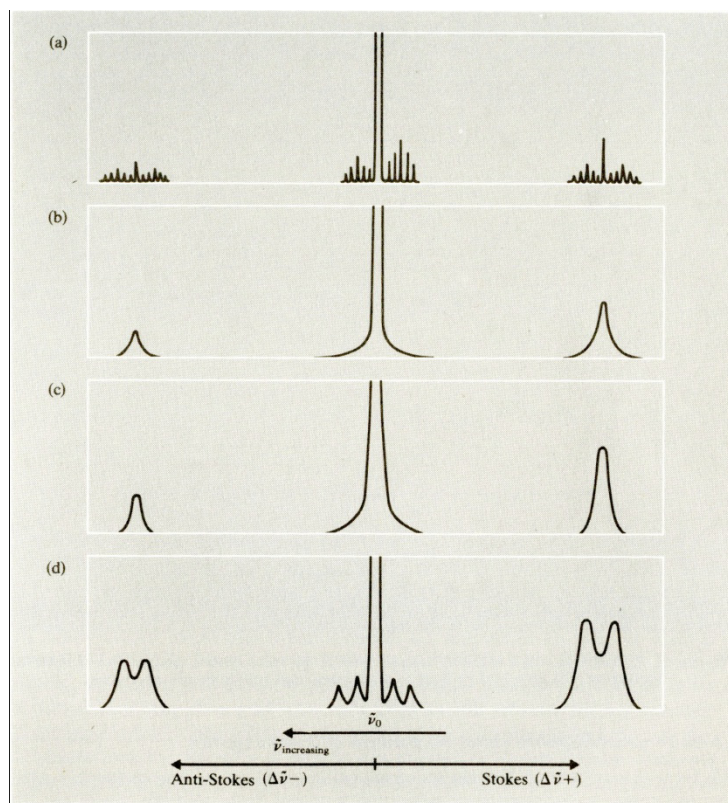


Figure 2-2

- (a) gas under high resolution, resolved rotation and vibration-rotation bands, (b) gas under low resolution, unresolved rotation and vibration-rotation bands, (c) Liquid, vibration bands, and (d) crystal, splitting of vibrational bands and stokes and anti-stokes libration bands. Adapted from [7]

For example, in an assembly of free molecules when we neglect electronic transitions and taken that the resolving power is large enough, Raman spectrum will be a series of finely spaced lines of relatively small wavenumber shifts which are arising from the rotational level transitions in the vibrational ground state. Also it will have a number of other lines of larger wavenumber shifts, arising from transitions with either a change of vibrational state and or a simultaneous change of vibration and rotational states. The Stokes and anti-Stokes Raman lines of rotational levels will have similar intensities because of the small separation of the rotational energy levels in rotational levels. On the other hand, Raman lines appeared because the change in vibrational states possess a much weaker intensity

of anti-Stokes peaks as compared to Stokes except for relatively small values of Raman shift ν_m . With moderate resolving power the gas Raman spectrum shows only vibrational transitions, and more finely spaced lines of rotational quantum number will not appear. They will more or less look like unresolved wings appearing around the Rayleigh line for pure rotational transitions and around Raman lines of vibrational origin for rotational transitions which occur, with a change of quantum number as well. For liquids, no matter what the resolving power is, Raman spectrum will show only bands of vibrational origin and that is because in liquids free rotation is inhibited. The wavenumbers will usually appear with slight nuances as compared to the ones observed for the molecule in the gaseous state and the main reason for that is the environmental perturbation of the energy levels. The case of molecular crystals shows not only larger intramolecular wavenumber shifts but also additional smaller wavenumber shifts, which are a result of intermolecular motions, like translation and rotation of molecules relative to another. However, the environment symmetry in which the molecule is observed and also interactions between the molecules in a unit cell and some other factors can result in the observation of still further bands. As a result, the Raman spectrum strongly depends on the symmetry and the crystal symmetry interactions' strength and the Raman spectra complexity in crystals as compared to liquids is matched with its rich information content.

3. Graphene

This single molecule crystal of carbon atoms is the building block for all of the carbon allotropes. It has been studied for 60 years theoretically before its experimental

discovery in 2004 and has won the Nobel Prize in physics for A. K. Geim and K. Novoselov.

3.1. Structure

Monolayer graphene unit cell is a lozenge containing two A and B atoms. Each of them forms a triangular 2D network and has a separation of $a_c = 0.142$ nm.

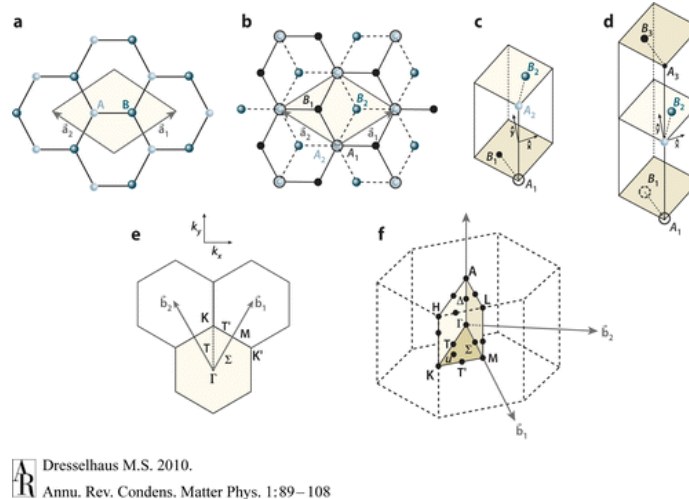


Figure 3-1

Graphene unit cells (a) monolayer graphene, (b) bilayer graphene, (c) bilayer graphene, (d) trilayer graphene, (e) 1st Brillouin zone with its high symmetry points and lines, and (f) The Brillouin zone for 3D graphite, showing the high symmetry points and axes. Adapted from [3]

Bilayer graphene is the result of stacking two of these planes in a way that the vacant center of one of the hexagons on the top network is occupied by the carbon atom on the lower plane. Usually, the stacking of more than three layers of graphene but less than 10 layers is called few layer graphene. For more than 10 layers, it becomes difficult to distinguish graphene from graphite. The structure has been confirmed to be hexagonal by Meyer et al. Using TEM.^[6] Ripples with a magnitude of up to one nanometer are observed in a graphene sheet. Whether it is an intrinsic property or an extrinsic property caused by impurities close to graphene sheets still remains to be studied. Finally, edges in

graphene play an important role since they are one of the main defect origins. An edge represents an irregularity in the infinite 2D structure and thus by breaking the symmetry increases the defect-induced Raman signal. It is worthy of noting that armchair and zigzag edges possessing different electronic properties contribute differently to Raman signal.

3.2. Properties

3.2.1. Mechanical

The sp^2 carbon-carbon bond is the strongest ever measured. It is supposed to have superior mechanical properties. In order to define the mechanical properties we will need to have Young's modulus E representing the stiffness, Poisson's ratio ν , and the shear modulus G . Lee et al.^[8] reports Young's modulus of 1 TPa, Third order elastic stiffness $D=-2$, and intrinsic strength of 130 GPa for graphene. Poisson's ratio have been reported ranging between 0.149 and 0.45, and G from 0.21 TPa to 0.408 TPa.

3.2.2. Electronic

Graphene is a near perfect electronic conductor because it has a zero-gap, and also because ballistic transport has been observed in graphene sheets. In ordinary conductors that we encounter in our everyday life, charge carriers are scattered during their movement through material, and in effect they will lose their momentum. In graphene, however, charge carriers can move as far as 0.3 micrometers without losing their momentum and being scattered. This phenomenon is called electronic ballistic transport. Their concentration can be modified as high as 10^{13} cm^{-2} , and their mobility $15000 \text{ cm}^2\text{V}^{-1}\text{s}^{-1}$ under ambient conditions, even on physically and chemically doped devices.^[9]

3.3. Synthesis

There are several reported ways to produce graphene. Micromechanical cleavage of graphite is the one usually used to produce monolayer graphene, Other procedures such as exfoliation and growth tend to produce multilayers. Graphene used to be prepared by exfoliation of HOPG (highly oriented pyrolytic graphite), which is a synthetic bernal stacked graphite acquired from carbon precursors and heat treated at over 3200 °C and under pressure. There are also records of preparing graphene on a nano-diamond precursor material. Both of two methods result in multilayer graphene. Another way of getting graphene samples is using a SiC-based precursor method, leading to a graphene family of materials which has significant interaction with the SiC substrate. Hence, they will show different properties like only partial stacking order. Epitaxial chemical vapor deposition (CVD) growth of graphene can also be done with transition metal catalysts, such as Ni, and this field is still under development.^[3,9]

3.4. Characterization

There are several characterization methods which could be used to detect graphene on a surface among which are optical observation and microscopy, Raman spectroscopy and atomic force microscopy.^[9]

3.4.1. Optical observation and microscopy^[6]

Monolayer graphene sheets are usually accompanied by a bigger portion of thicker flakes. On most of the substrates the graphene sheets cannot be detected, and that is what makes the choice of the substrate for observation so vital. They only become visible when they have been deposited on a Si wafer with a delicately modified layer of SiO₂ on it. The thickness of oxide layer should be around 300 nm. In this case, even a monolayer

adds to the optical path just enough, to change the interference color with respect to the empty substrate.

3.4.2. AFM/STM^[6]

Atomic force microscopy was the only method to recognize single and few layer of graphene before Raman spectroscopy. One of the problems of using this method was the low through put. Also, because of the chemical contrast between the graphene and the substrate, practically it is only capable of distinguishing between monlayer and bilayer graphene if films have folds and wrinkles. This is a drawback preventing the widespread usage of this method.

3.4.3. Raman Spectroscopy

Ferrari et al.(2006)^[2] demonstrates that graphene's electronic bonding structure can be uniquely recorded in Raman spectrum. Since this method allows high-throughput, nondestructive identification of graphene layers, it seems to be the best way to approach the problem of characterization of graphene. Therefore, this research uses Raman spectroscopy as a primary analytical tool to study graphene under high pressure.

4. High Pressure equipment: Diamond Anvil cell (DAC)

The high pressure experiments are made in a gasketed Diamond Anvil Cell (DAC). This simple technology device consists of two apposed Anvils (made of single crystal diamond, sapphire, zirconia or moissanite) which pass external forces onto metal gasket in between the anvils. A small hole is drilled at the center of pre-indented gasket for sample chamber. A sample, pressure marker (e.g. ruby chips) and pressure transmitting medium (a mixture of ethanol, methanol) are loaded in the sample chamber. The reachable pressure depends on the gasket material, dimension of the sample chamber,

culet size of the anvils, pressure medium and also cell structure. Different metals e.g. copper, rhenium, stainless steel and tungsten can be used as a gasket. The sample chamber diameter should usually be equal or less than half of the culet size for the pressure to reach as high as possible. Pressure measurement is usually done using ruby fluorescence method which has two important advantages: 1) it makes determination of pressure rather instantly making the in-situ measurements possible, and 2) it is sensitive to microscopic stress, making hydrostatic pressure checking possible through Raman peak broadening analysis.

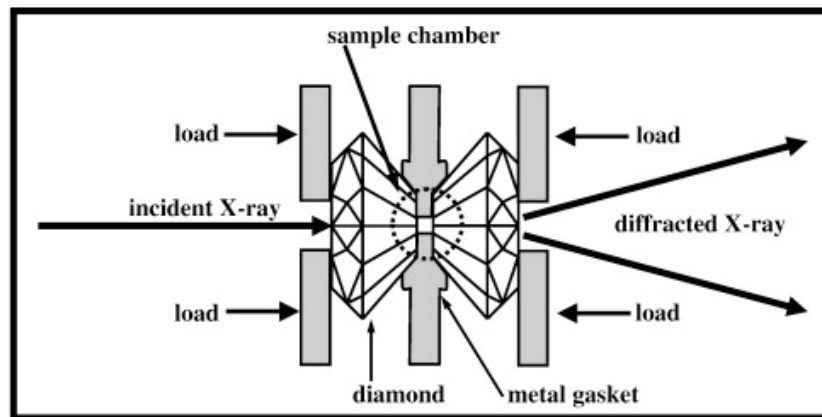


Figure 4-1
Schematic of a DAC adapted from[10]

Different types of cell are available for high pressure study. from which NBS cell, Basset cell, Mao-Bell cell, Syassen-Holzapfel cell, and Merrill-Basset cell could be named. The images show some of these cells.

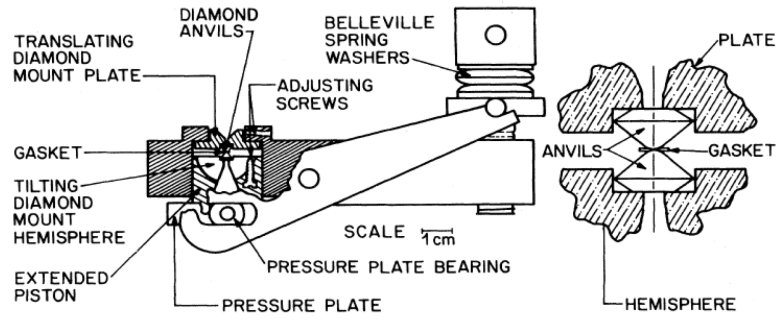


Figure 4-2
NBS cell developed by Piermarini and block 1975. Adapted from [11]

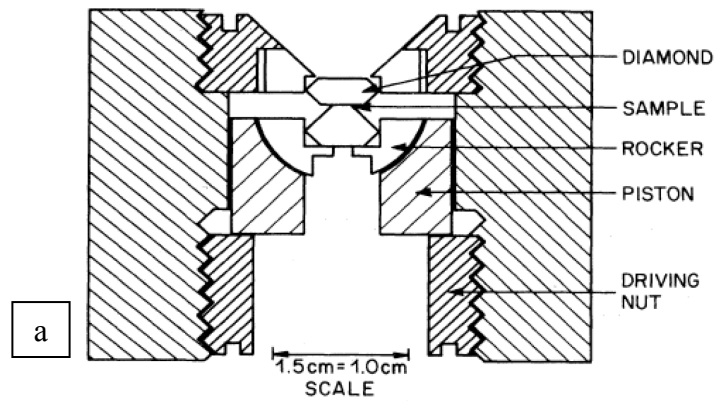


Figure 4-3

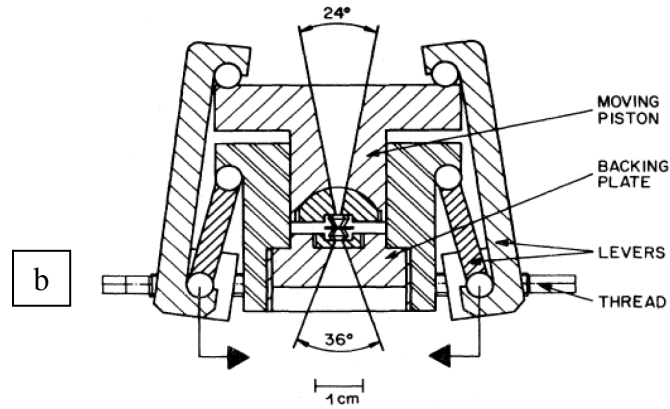


Figure 4-4
(a) Basset type cell. (b) Syassen-Holzappel cell Adapted from [11]

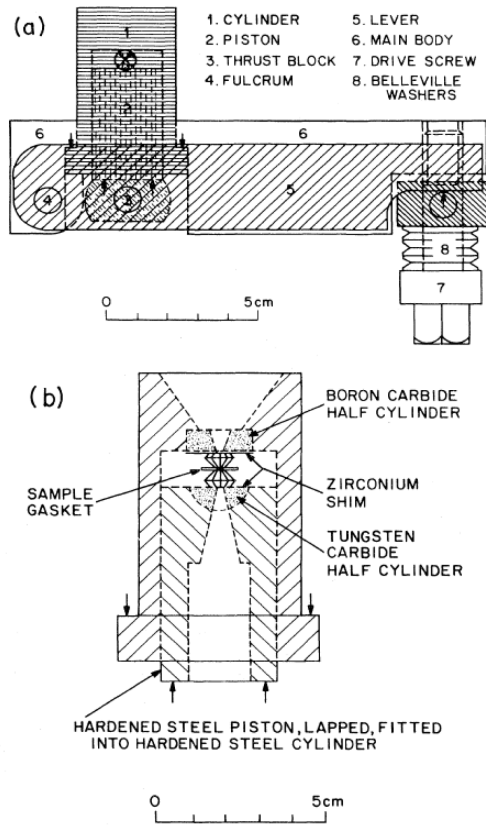


Figure 4-5
 (a)Mao-Bell cell Mao et al. (1978) (b) long cylinder-piston assembly with anvil diamonds set in carbide half cylinders. Adapted from [11]

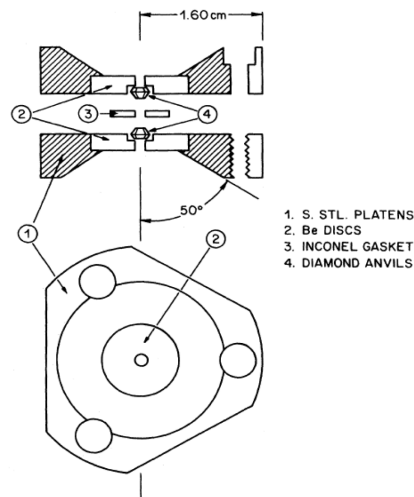


Figure 4-6
 Merrill-Basset miniature cell for X-ray studies(1974). Adapted from [11]

5. Equipment and Materials

5.1. Raman Spectroscopy Stage

As described in the previous chapter, Raman spectroscopy works in the basis of measuring the laser excitation response of the sample. The laser light passes a wavelength-selective beam splitter and shines on the sample through a microscope magnifying objective. Scattered beam is then collected with the same objective. It is going to be filtered once more by the beam splitter and by a monochromator (a filter that eliminates most of the laser frequency, making the process easier). Then the beam goes to a spectrometer and changes into an electronic signal. The digitalized signals, i.e. Raman spectrum, are recorded on a computer. In our setup, laser beam is generated by an air-cooled Argon Ion laser system (spectra physics model 177, multi-line, maximum power: 400mW). The path of the excitation laser beam includes a prism, two mirrors, Pellicle beamsplitters (8R/92R), a 20X magnifying lens. The scattered light passes through the beam splitter again and then comes to the Holographic Imaging Spectrograph (Kaiser Optical Systems Holospec). Our system is also equipped with a camera which helps to select regions of interest on the sample for Raman spectrum. The scattered light can also be directed thorough a mirror into a fluorescent spectroscope for measuring the pressure using ruby scale. The ruby signal is then processed by software and provides the possibility of in-situ pressure measurement.

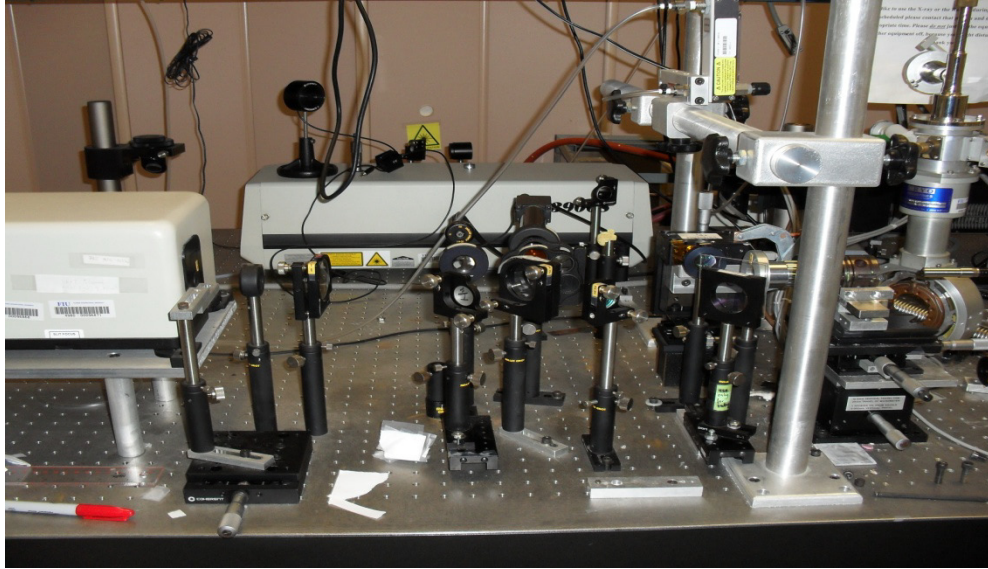


Figure 5-1
cesMEC Raman stage

5.2. Anvils

Anvils used for this research are made of single crystal diamond anvils and zirconia anvils.

5.2.1. Diamond Anvils

Since a wide range of pressures can be reached using diamond anvils it has been the device of choice for high pressure-temperature researches. However, the diamond anvils are expensive and the methodology is considered somehow specialized.^[12] The pressures attainable with the Mao-Bell type DACs reached 50 GPa in 1975 and increased to hundreds GPa subsequently. We used DAC to reach around 9 GPa, which is easily attainable with diamond anvils. But the problem of using diamond anvils in our experiment was that there is a sharp diamond peak overlapping D peak of graphene, disallows the study of the D peak change in shape and position. So it was decided to shift to using zirconia anvils.

5.2.2. Zirconia Anvils

When Cubic zirconia (CZ) and moissanite are much less expensive compared to diamond. Their similar transparency, extreme hardness and superior high temperature stability make them good candidates for high pressure anvil, although they are restricted to lower maximum pressures than diamond anvils. Another advantage of CZ anvils is their good performance in IR and Raman spectroscopy, and it is worthy of noting that high wavenumber regime poses a low flat background signal from the CZ anvil.^[12] The most important reason that CZ anvils are preferred over diamond is the absence of the Raman peak, where D-peak of graphene is located. The attainable pressure using CZ anvils has been reported up to 15 GPa with a culet size of ~400 microns.^[12]

6. Results and discussion

6.1. Introduction

This research initially was aimed to investigate the gas adsorption properties of graphene (mainly Hydrogen). Plasma treated graphene's ability to absorb Hydrogen with a relatively high capacity has been reported by Dr. Koratkar's Group at Rensselaer. This new graphene can store 14 percent by weight Hydrogen at room temperature, which is far more than any other recorded material. Keyvan Rafiee, one of the researchers in Dr. Koratkar's group, agreed to send some of their samples. TEM images from the samples come below. Initially our intention was to investigate the Hydrogen storage capacity of the plasma treated graphene flakes and compare them with the untreated samples by a volumetric Sieverts apparatus. Unfortunately we could not get other labs to collaborate. So it was decided that maybe if we can just figure out how the plasma treatment changes the nature of the graphene we can have a stand point to do the comparison. A means to

achieve this would be Raman spectroscopy. Even if we cannot use the acquired data to have a measure for the gas adsorption comparison, it would be useful to know how the chemical bond strength will change after plasma treatment.

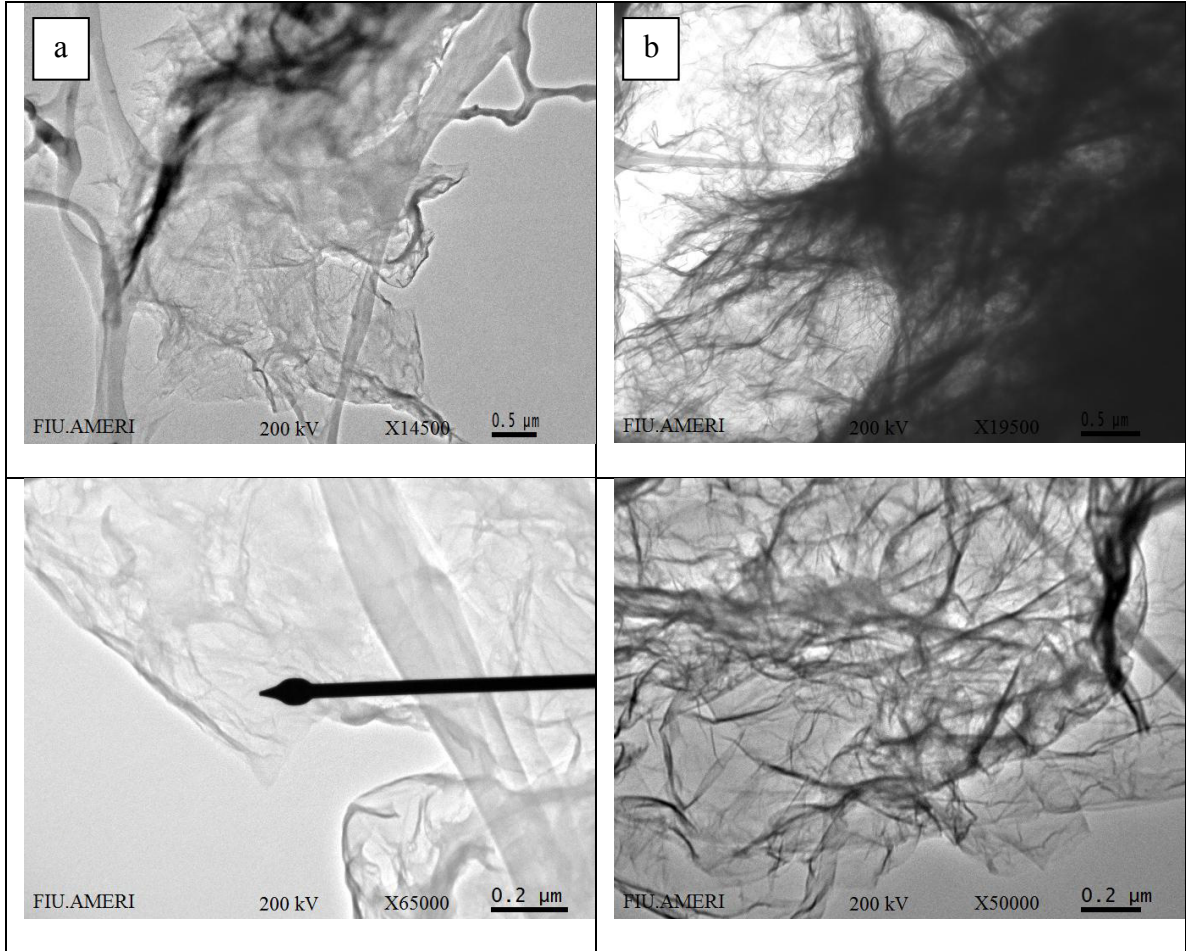


Figure 6-1

TEM images of the samples we got from the samples we received from RPI (a) graphene flake not treated magnified 14500X top and magnified 65000X bottom (b) Plasma treated graphene flakes 19500X top and 50000X bottom

6.2. Raman spectroscopy of Samples loaded into DAC

The 6"x6"x54 μ copper foils supplied by Nimrod Hall were punched into 100 μ and 250 μ pieces using a KEKO punching machine. Graphene film was synthesized by Chemical Vapor Deposition (CVD) of hydrocarbon on punched copper foils. This is how our collaborators in Dr. Choi's group, Santanu Das, has grown the graphene on the

prepared Cu foil. As they mention in [13]: “Copper foil was first annealed at 1000 °C for 1 hour under Ar atmosphere followed by acid-treatment for 10 min using 1 M acetic acid at 60 °C. Subsequently Copper foils were thoroughly washed with de-ionized water and dried at the ambient conditions. Furthermore Cu substrates were placed inside a 2” quartz tube of thermal CVD system. In short, graphene on the Cu foil was synthesized at 1000 °C and 1 atm pressure, using a 5 min flow of CH₄ and H₂ gases in 1:4 ratios. After graphene growth, the foil was cooled down to room temperature before being taken out from the furnace.”^[13]

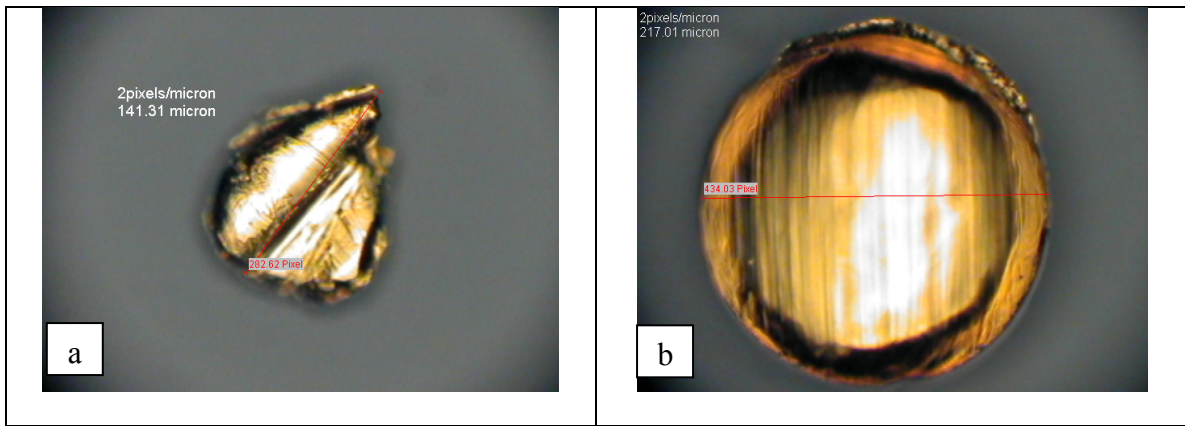


Figure 6-2
Copper foils before Graphene growth (a) 141.31 μ Cu foil (b) 217.01 μ Cu foil

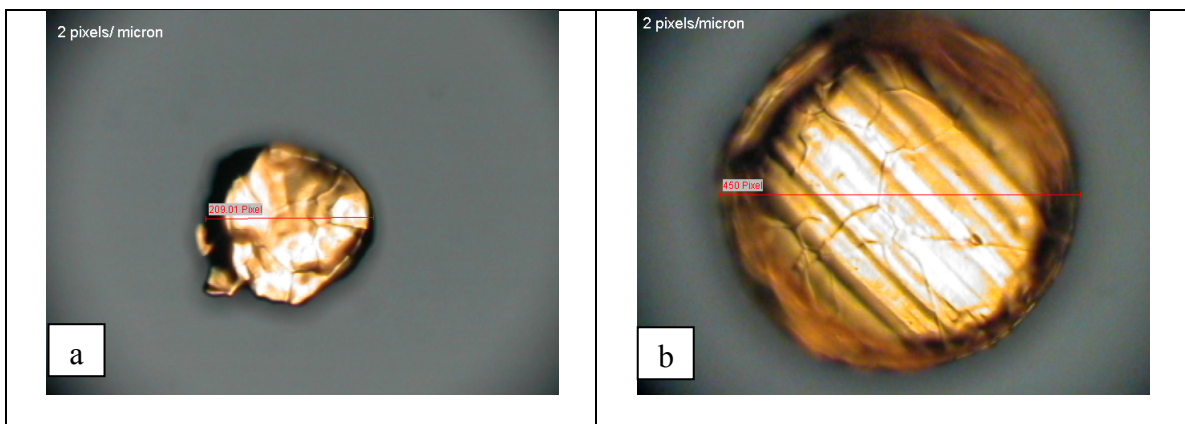


Figure 6-3
Copper foils after Graphene growth (a) 104.5μ (b) 225μ

Sample chamber was a hole of 150-200 μm in diameter and 60-80 μm in thickness (after pre-indentation) in the stainless steel gasket. Ruby chips were loaded in the sample chamber in order to give us a scale to measure the pressure by following the ruby peak position. A mixture of ethanol methanol was used as pressure medium. The existence of the graphene was confirmed using Raman spectroscopy before increasing the pressure. The pressure was increased step by step and the Raman Spectra was recorded in each of these steps. Then the high range and the low range spectrum were separated in an excel worksheet. After eliminating the background and using FITYK to fit the peaks, the following diagrams were obtained.

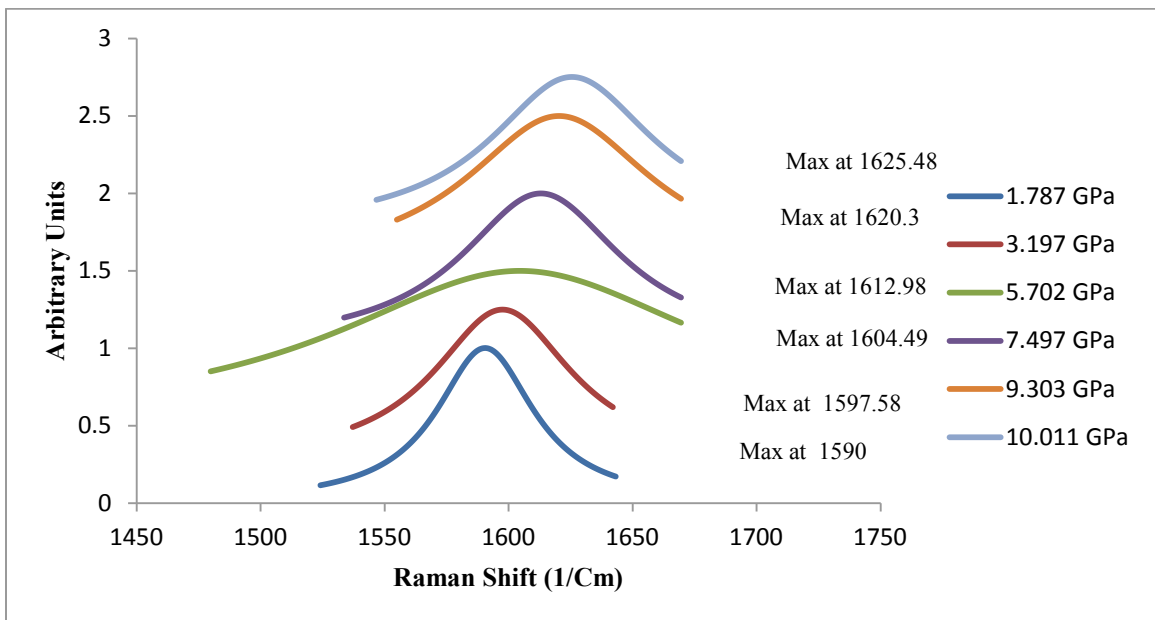


Figure 6-4

Figure shows how G band peak position changes when pressure is increased. And indicates how the fitted peaks look like. The Y axis does not show the real intensities

It seems that increasing pressure does not affect the position of 2D band as much as it does in the case of G band. D band overlaps the diamond peak, and so it could not be studied. Also, further studies with free standing graphene which will not have the large copper background could improve the results. However, the main purpose of this research is to compare the Raman spectra of plasma treated graphene with non-treated graphene. Future studies will focus on putting the plasma treated graphene in DAC and to compare it with the current results.

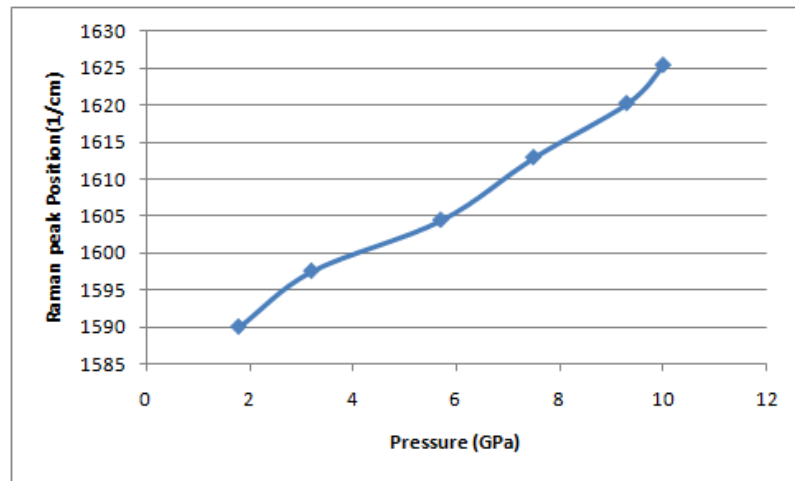


Figure 6-5

After fitting experimental results for Raman spectroscopy of few layer graphene show that G band peak position changes almost linearly with pressure increase.

The same diagrams can be plotted for 2D band with the same method. For 2D case the peak seems to be better consistent with a doublet peak. The change with pressure increase is much less and more scattered, which might be due to the experimental error.

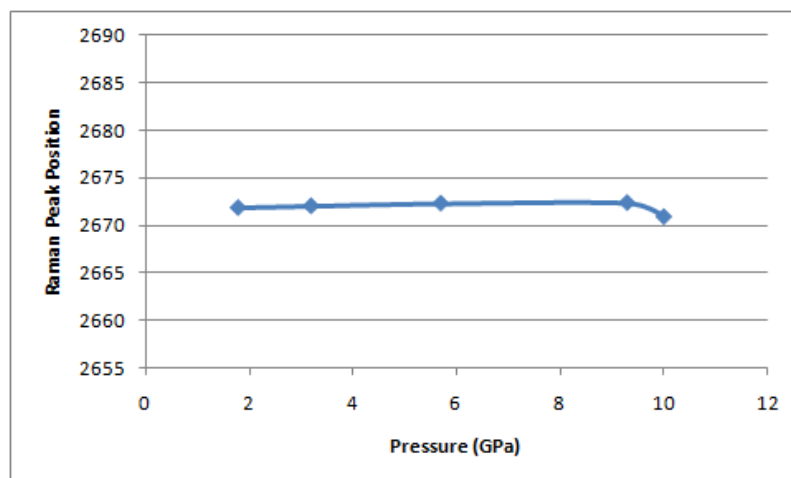


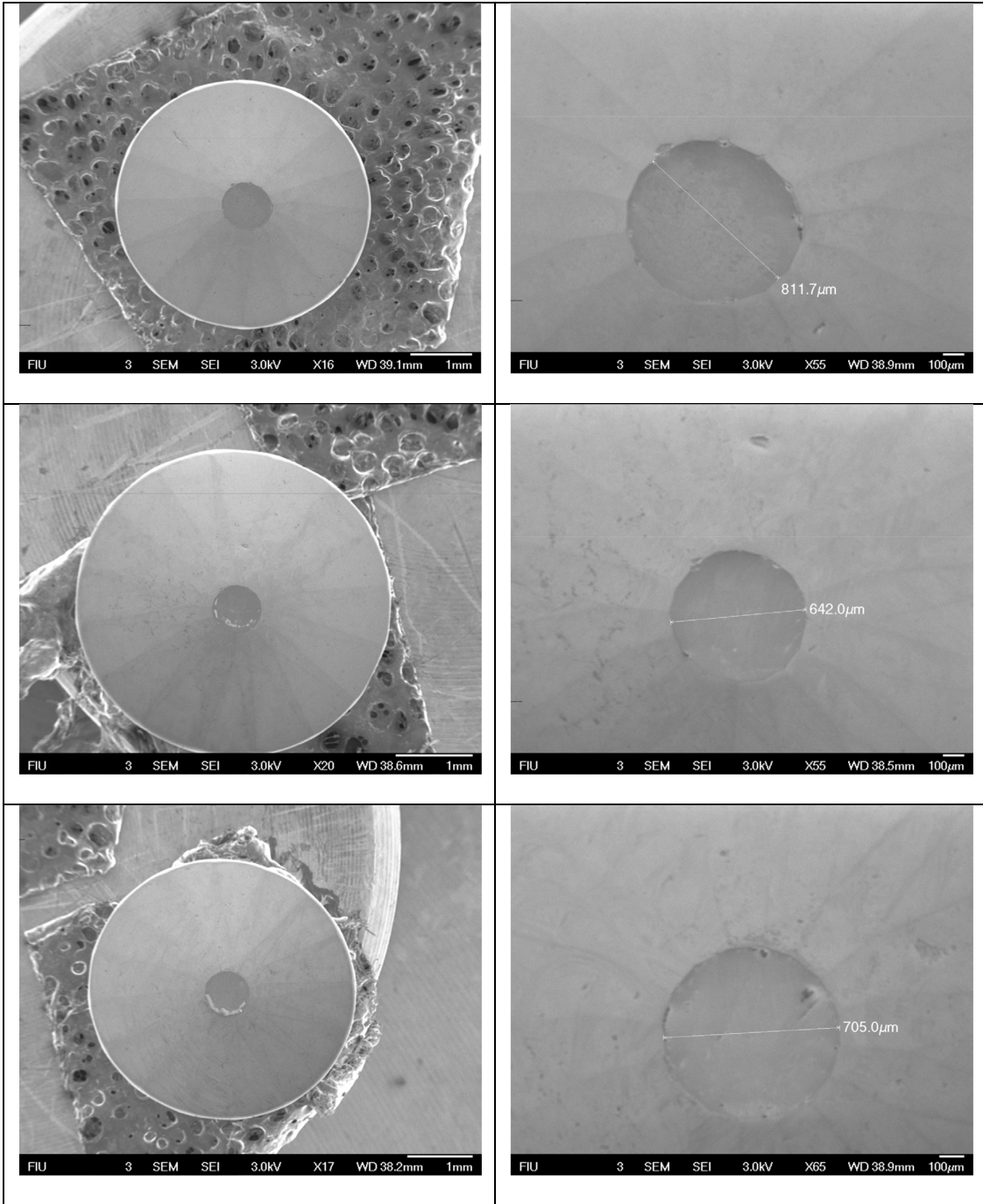
Figure 6-6

After fitting experimental results for Raman spectroscopy of few layer graphene shows that 2D band peak position does not change drastically with pressure increase.

Since in the run with the diamond anvil the D-peak was not detectable, it was decided that Zirconia anvil might be a better candidate to be used instead of Diamond anvil. This way the maximum attainable pressure would be less, but we hoped this way we will be able to detect D-peak better, which unfortunately turned out to be wrong and will be described in the following section.

6.3. Raman spectroscopy of Samples loaded into ZAC

50 cubic Zirconia gems were loaded in SEM and sorted by diameter size with 2 digits precision. Then during the Raman runs gems with the closest diameter size were chosen in order to get better results. Some of the SEM images taken while sorting the gems come below.



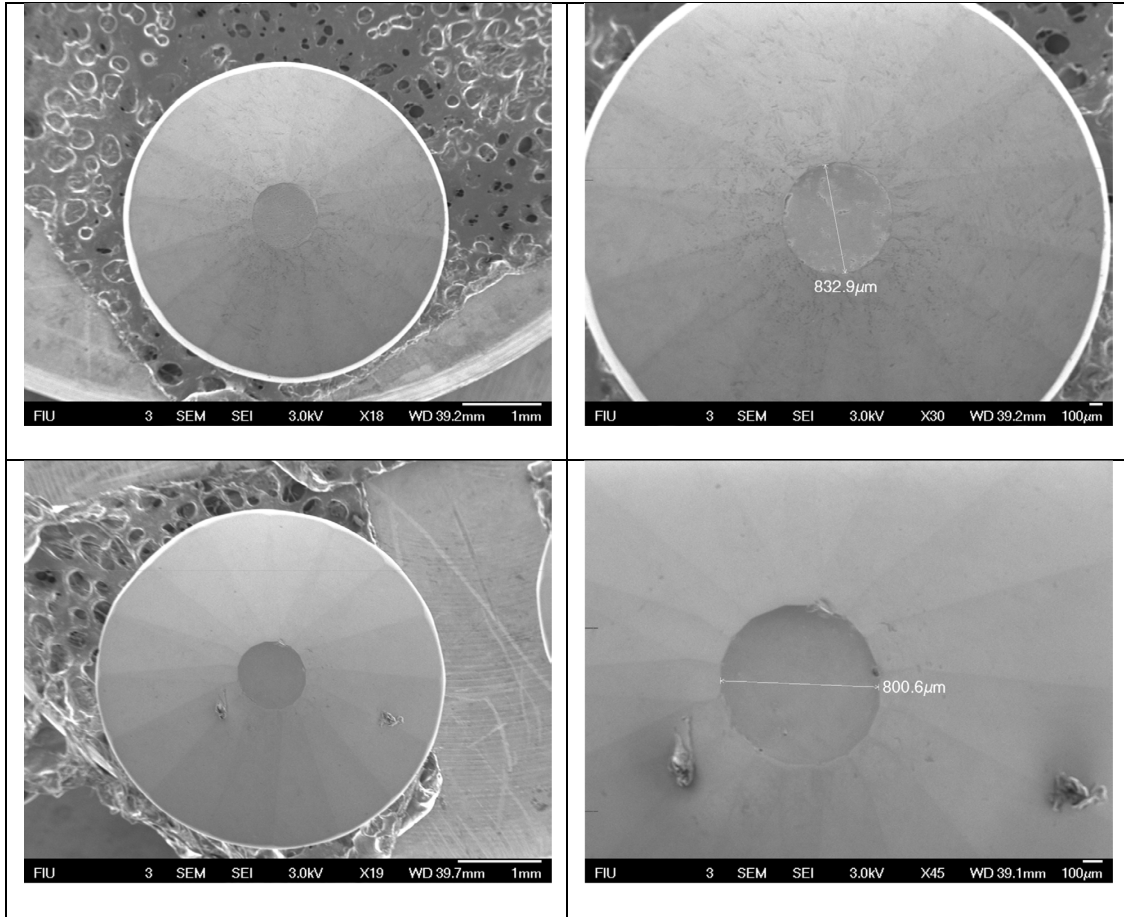


Figure 6-7
SEM images taken from the Zirconia gems

Meanwhile precautions were taken in order to make sure that gems with defects on them are not going to be used to increase the attainable pressure as much as possible.

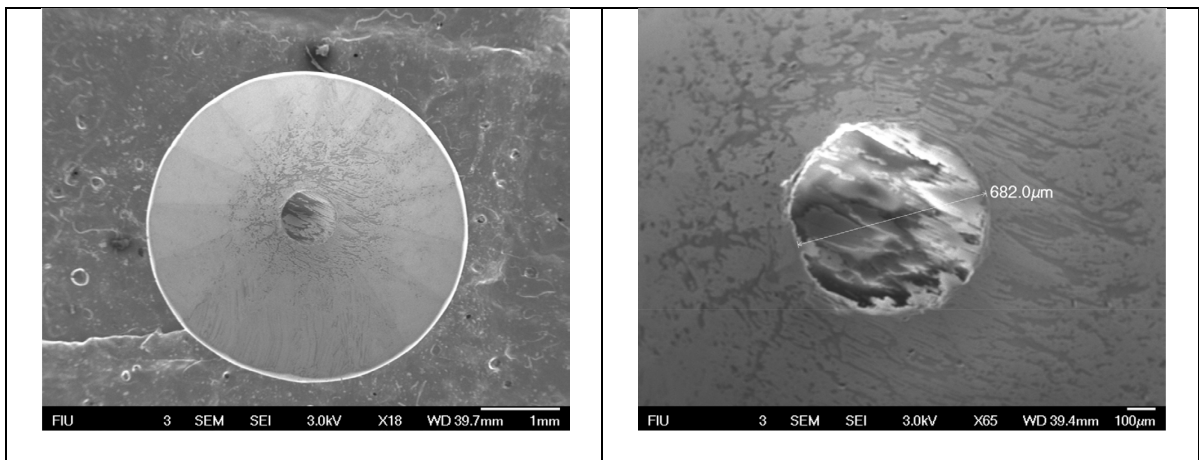


Figure 6-8
Sample of a defective gem

The range of culet size change was found to be from 680 μ to 1035 μ . This range of culet size seems to be too large so we cannot expect to reach the upper limits of pressures which, has been recorded by using zirconia anvils. After sorting the gems by size, one the problems which needs to be addressed is that when working with zirconia anvils, the anvils are usually good for one run and then they will break and there is a need to change the anvils after each run. In mostly all of the usual cells which are being used for reaching high pressure (Mao-Bell, Basset and etc) there is a need to glue the anvil to the seats and glueing is a time consuming process. After making the glue it should be applied evenly between the seat and the anvil and then should be left to dry for half an hour. Afterwards the seat should be placed in the furnace for almost 3-4 hours. This means even before starting the alignment process each time, it takes around 6 hours to prepare the cell. In order to avoid glueing the gems each time and to facilitate the process it was decided to use a cell which was manufactured in ceSMEC machine shop for the hydrogen loading system. The advantage of this cell over commonly used cells is that with this device the anvil can be screwed to the seat using a metal plate which mounts on the gem and has an opening for the laser light to enter. Furthermore for adjusting the tilt three screws can be used which are devised to tilt one of the seats to make both of the culets exactly parallel.



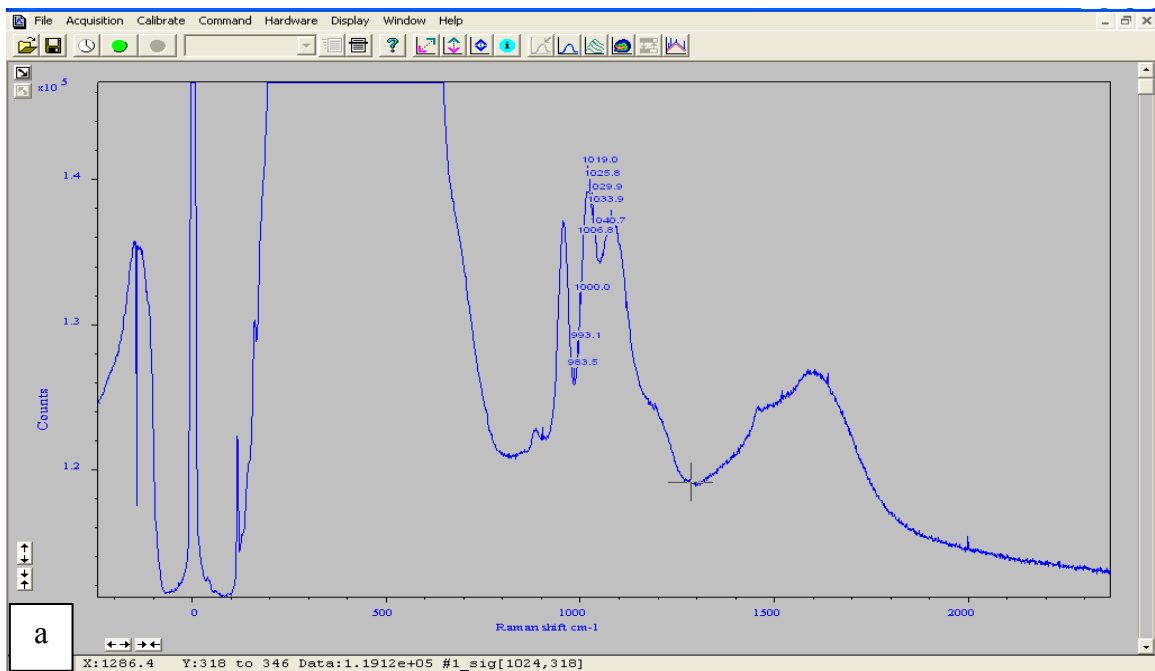
Figure 6-9
Diamod anvil cell made in CeSMEC machine shop

Again the 6''x6''x54 μ copper foils supplied by Nimrod Hall were used to be punched by the KEKO punching machine. This time they were punched into 150 μ pieces to get better results. Because judging by the last run with DAC 250 μ seemed to be too large for the sample chamber and 100 μ pieces remained attached to the surface of the copper foil and for detaching them the foil needed to be scratched. The resultant pieces had a deformed shape and were beveled which might cause complications for the graphene grow process. The 150 μ pieces came off the copper foil on their own and since there was no need to scratch the surface their shape was not as distorted as 100 μ pieces were. After punching the foils and gathering the pieces, they were dispersed with acetone on small ceramic disks(d~1.2cm) and then delivered to Santanu for Graphene growth. After graphene existence was confirmed by Raman Spectroscopy, they were again submitted to Santanu to be plasma treated with different partial pressures. They were treated with partial pressures ranging from 75 m Torr up to 175m Torr and power 50w, gas flow 5sccm, and 30s time. Now the samples being ready to be loaded into the cell, gems should be mounted and then aligned. After aligning the gems the tilt should be adjusted using the Newton rings. Tilting the adjustable seat should be done in order for the newton rings to disappear. A gasket should be made out of a suitable metal. It was decided that the gasketing material for the CZ anvils would have to be far softer than the common gasketing materials used with diamonds. Therefore, copper was chosen as the gasket material and worked fine at supporting the anvils but sometimes was proven problematic at sealing liquid into the cell. The copper foil thickness is around 760 μ and it will be fixed using two screws designed for the aforementioned purpose on of one the seats. Then it will be indented until the thickness is less than 100 μ . After indentation it is time

to make a sample chamber in order to load the sample. Using a Betsa Electric Discharge Machine (EDM) a hole of around $270\ \mu$ is drilled in the center of indented area which acts as the sample chamber. Then the gasket is sonicated with acetone and dried. After completely drying the sample it will be fixed to the seat again. Measurements are taken for the gasket to be screwed exactly on the same place it was indented because indented edges are not exactly symmetric. Then the using a used Omniprobe tip which is attached to a Pin Wise the graphene grown pieces of copper will be transferred to the sample chamber. The ideal case would be to take the side of the sample to make sure the thin layer of graphene on it will not be removed and then transfer it to the sample chamber on the same side which is a hard task due to the small nature of the sample, and sample chamber. And also it is usually hard to contact the Omniprobe tip to the side of a 0.1 mm copper piece in a way that it holds on without flipping of the sample. After loading the sample a small ruby chip should be loaded into the sample chamber for the pressure measurements. In order to have hydrostatic pressure all over the sample chamber after all is in order, a drop of methanol:ethanol:water 16:3:1 was put on the sample chamber which will act as the pressure transmitting medium. Another problem which sometimes surfaced with the use of the softer CZ anvils was that, CZ was proved to be too soft for use with ruby chips. Sometimes with application of pressure to the CZAC, a shift was observed in the ruby R1 fluorescence, but with subsequent pressure applications no further shifts were observed. The ruby was gouging out holes in the CZ faces.

Then the cell is closed down and is transferred to be mounted on the Raman setup. The first step is finding and focusing on the sample which is inside the sample chamber then the pressure at initial step will be determined using the ruby. For achieving this goal the

laser beam should be placed on the ruby then the reflected beam will be collected and will be analyzed by the software. Then using the ruby peak position the pressure could be decided by a pressure table. Afterwards the pressure will be increased. Again by aiming the laser beam on the ruby the pressure will be decided and data collection at the new pressure will be started. This process will continue until one of the gems is broken, or the ruby is lost. At the next step the laser beam will be placed on our sample and the sampling for 10 min will start.



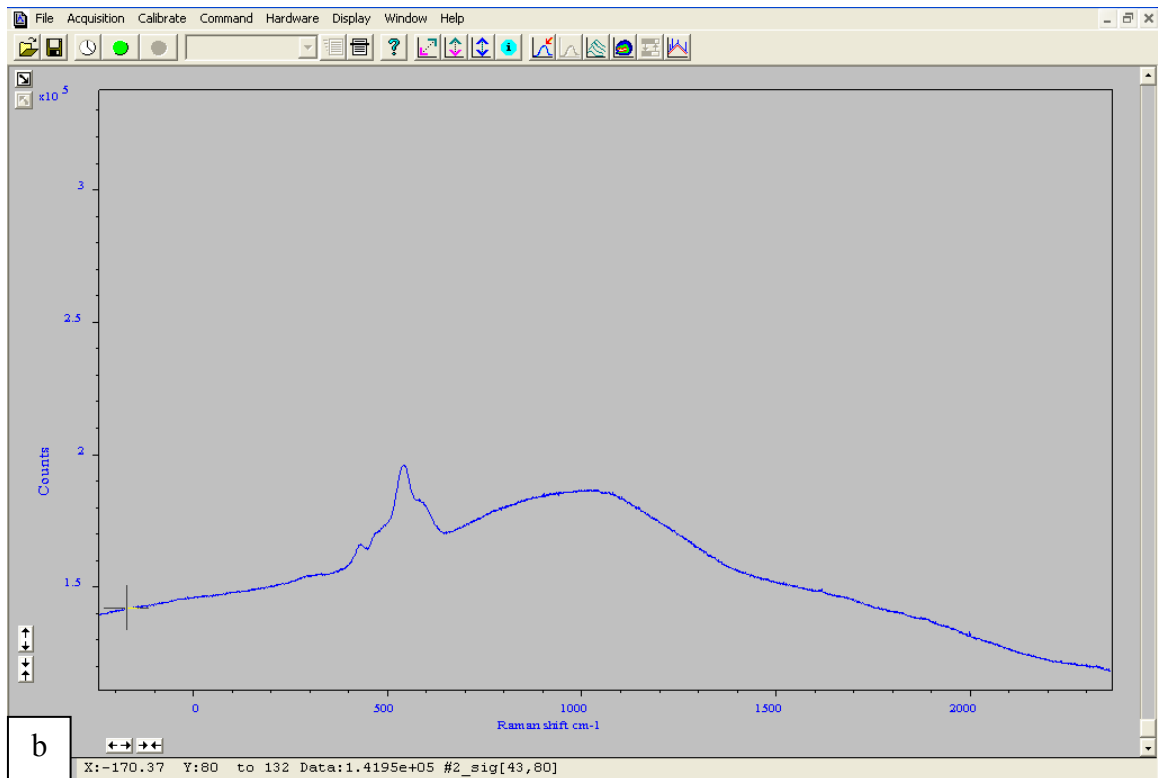


Figure 6-10

Sample Raman spectrum of plasma treated graphene taken by Andor software ruby peak at 695.03, partial pressure 100 (a) low range(-242_2364 cm^{-1}), (b) high range(2267_4553 cm^{-1})

After getting the data it would be saved in American Standard Code for Information Interchange (ASCII) format to be separated into two high range and low range spectra by a program developed in MATLAB for this purpose. Then the ranges which contain irrelevant high intensity peaks are eliminated. These peaks which do not belong to graphene make the detection of graphene peaks in the spectra almost impossible.

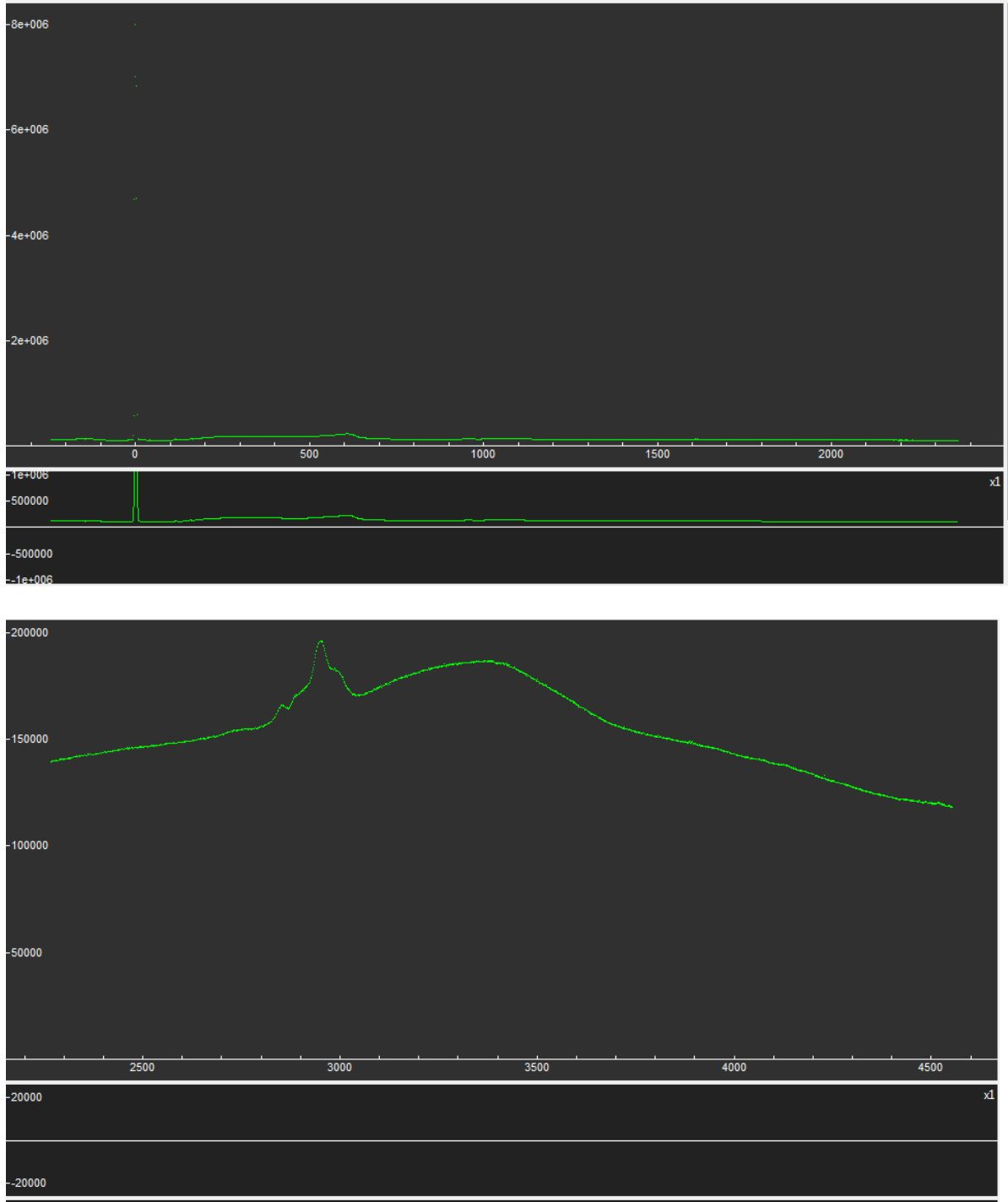


Figure 6-11
 Raman spectrum of plasma treated graphene by FITYK software ruby peak at 695.03, partial pressure 100. (a) low range(-242_2364 cm^{-1}), (b) high range(2267_4553 cm^{-1}). As can be observed without elimination of the large peaks(like the one at 0 which belongs to Rayleigh scattering) smaller peaks related to graphene are not visible

Usually the range chosen for processing the Raman data is from 1000-2000 cm^{-1} for low range which contains the D-peak \sim 1320 cm^{-1} and G-peak \sim 1580 cm^{-1} and 2000-3000 cm^{-1} for the high range which contains the 2D-peak (G'-peak) \sim 2640 cm^{-1} . Then using FITYK the background will be eliminated. Then the peaks are being fitted using the same software. Levenberg-Marquardt method and Lorentzian function were chosen to fit the peaks. After fitting each spectrum the peaks which were close to graphene peak positions were chosen and their position change by increasing pressure was tracked. The obtained results come below:

6.4.1. Partial pressure 75 mTorr

Low Range

Pressure(GPa)	Ruby peak position(1/cm)	Number of peaks used to fit	peak position	FWHM	HWHM
0.13	694.77	5	1622.44	174.234	87.12
0.26	694.9	5	1623.46	183.567	91.78
0.65	695.29	5	1619.76	182.151	91.08
0.77	695.41	7	1624.73	201.219	100.61
1.03	695.67	6	1611.33	185.6	92.8
1.29	695.93	5	1624.94	173.91	86.96
1.42	696.06	5	1621.41	194.11	97.06
1.67	696.31	5	1625.5	161.4	80.7

Table 6-1

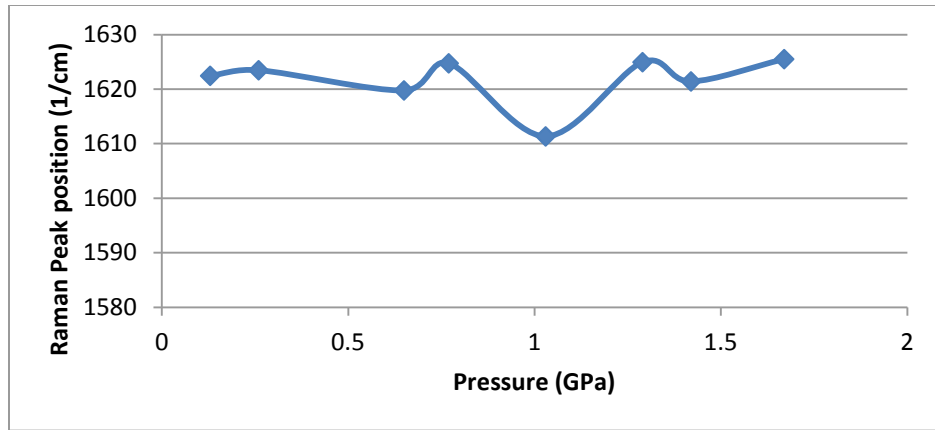


Figure 6-12

High Range

Pressure(GPa)	Ruby peak position(1/cm)	Number of peaks used to fit	peak position	FWHM	HWHM
0.13	694.77	8	2698.47	82.26	41.13
0.26	694.9	10	2704.62	365.1	182.55
0.65	695.29	5	2675.88	117.16	58.58
0.77	695.41	5	2737.15	102.891	51.45
1.03	695.67	5	2703.19	53.11	26.55
1.29	695.93	5	2741.74	271.45	135.73

Table 6-2

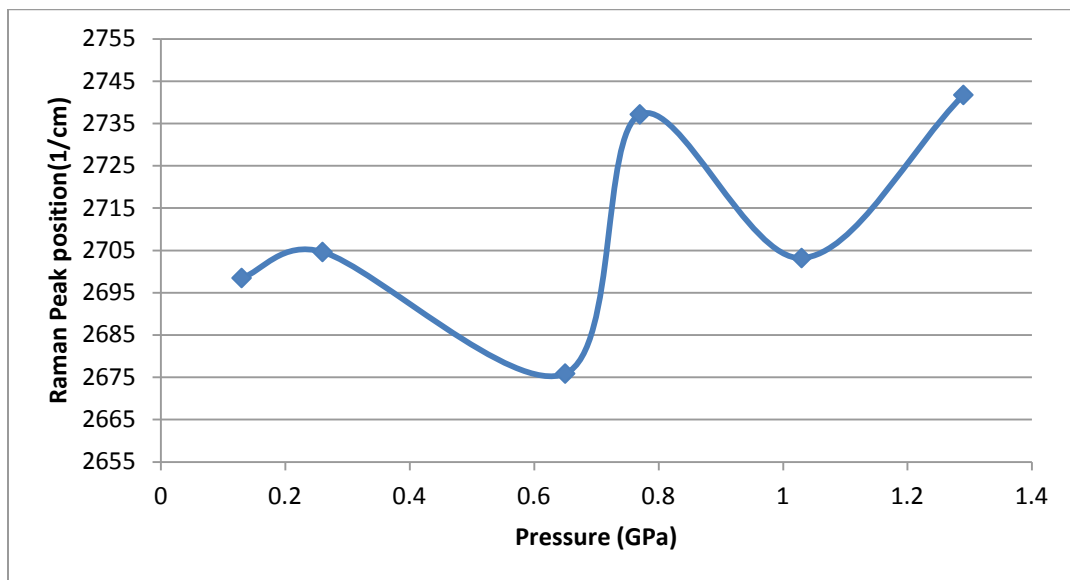


Figure 6-13

6.4.2. Partial pressure 100 mTorr

Low Range

First background reduction

Pressure(GPa)	Ruby peak position(1/cm)	Number of peaks used to fit	peak position	FWHM
0	694.64	6	1619.05	126.153
0.13	694.77	6	1630.57	150
0.39	695.03	8	1637.54	140.203
0.65	695.29	6	1643.51	109.958
0.77	695.41	9	1639.89	168.212

Table 6-3

Second background reduction

Pressure(GPa)	Ruby peak position(1/cm)	Number of peaks used to fit	peak position	FWHM
0	694.64	6	1618.13	119.723
0.13	694.77	6	1631.85	108.514
0.39	695.03	8	1633.94	106.736
0.65	695.29	6	1645.31	113.803
0.77	695.41	12	1664.98	96.8

Table 6-4

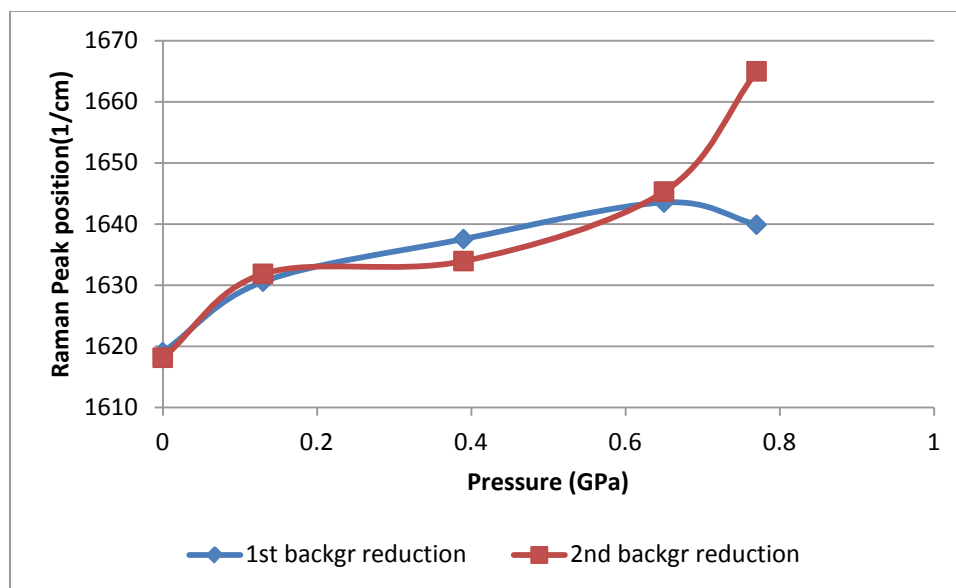


Figure 6-14

High Range

First background reduction

Pressure(GPa)	Ruby peak position(1/cm)	Number of peaks used to fit	peak position	FWHM
0	694.64	13	2686.48	148.99
0.13	694.77	10	2707.76	186.897
0.39	695.03	15	2707.51	138.03
0.65	695.29	8	2723.68	180.102
0.77	695.41	11	2710.74	185.5

Table 6-5

Second background reduction

Pressure(GPa)	Ruby peak position(1/cm)	Number of peaks used to fit	peak position	FWHM	HWHM
0	694.64	13	2669.2	117.207	58.60347
0.13	694.77	14	2727.2	72.8	36.40161
0.39	695.03	15	2721.12	90.5834	45.2917
0.65	695.29	14	2729.19	81.637	40.81878
0.77	695.41	11	2714.24	107.84	54.5

Table 6-6

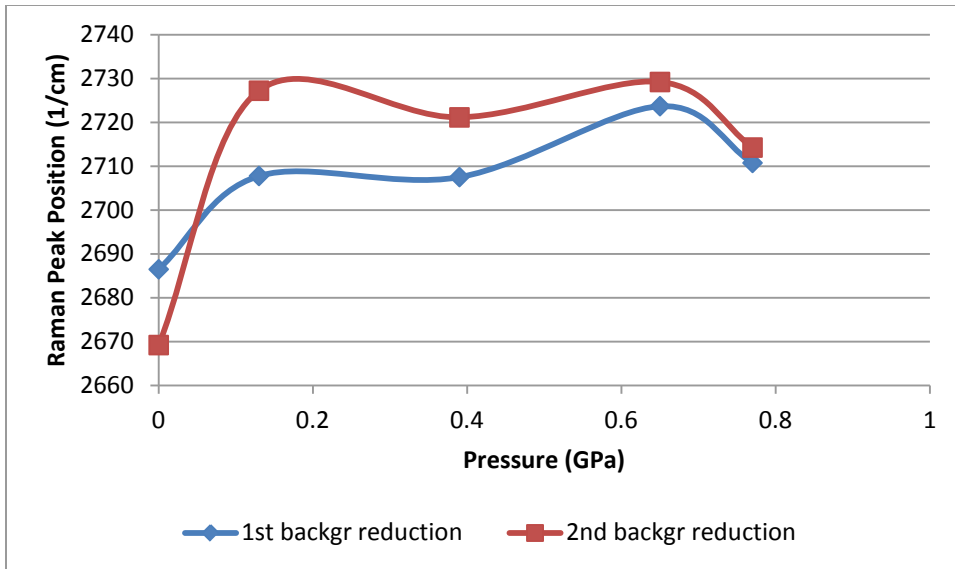


Figure 6-15

6.4.3. Partial pressure 125 mTorr

Low Range

First background reduction

Pressure	Ruby peak position	Number of peaks used to fit	peak position	FWHM	HWHM
0	694.64	8	1618.77	139.523	69.76147
0.26	694.9	9	1644.242	157.613	78.81
0.39	695.03	8	1644.75	163.3	81.65
0.65	695.29	11	1755.58	292.92	146.46
0.77	695.41	7	1622.04	142.96	71.48
0.9	695.54	6	1623.21	187.48	93.74
1.03	695.67	11	1658.13	173.28	86.64

Table 6-7

Yellow shade is where the result seemed uncertain it was not included in the graph

Second background reduction

pressure	Ruby peak position	Number of peaks used to fit	peak position	FWHM	HWHM
0	694.64	9	1615.7	184.161	92.08
0.26	694.9	8	1611.12	148.689	74.34
0.39	695.03	8	1640.94	121.33	60.567
0.65	695.29	20	1695.82	80.59	40.29
0.77	695.41	5	1623.46	122.133	61.07
0.9	695.54	6	1622.51	144.67	72.34
1.03	695.67	11	1643.03	181.21	90.6

Yellow shade is where the result seemed uncertain it was not included in the graph

Table 6-8

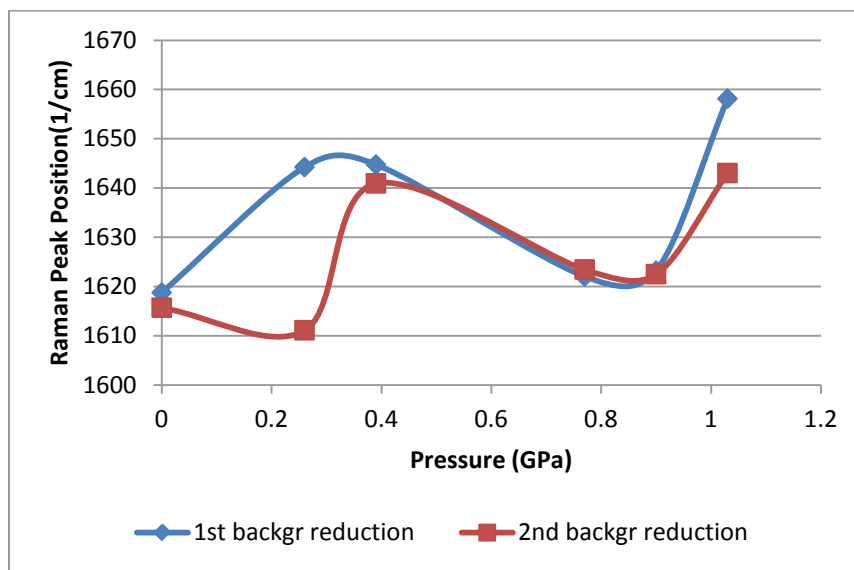


Figure 6-16

High Range

First background reduction

pressure	Ruby peak position	Number of peaks used to fit	peak position	FWHM	HWHM
0	694.64	5	2711.976	92.08	46.04
0.26	694.9	6	2709.176	169.896	84.95
0.39	695.03	23	2717.353	0.20804	-0.10402
0.65	695.29	49	2706.81	2.76	1.38
0.77	695.41	28	2679.823	0.2276	0.1138
0.9	695.54	43 (no peaks detected)			
1.03	695.67	31	2677.38	0.3806	0.1903

Table 6-9

Second background reduction

pressure	Ruby peak position	Number of peaks used to fit	peak position	FWHM	HWHM
0	694.64	5	2706.62	84.88	42.44
0.26	694.9	6	2712.39	126.895	63.45
0.39	695.03	23	2717.33	0.186266	-0.93133
0.65	695.29	40	2707.27	1.53	0.763
0.77	695.41	28	2703.56	0.3812	0.1906
0.9	695.54	43 (no peaks detected)			
1.03	695.67	31	2677.37	0.183958	0.09198

Table 6-10

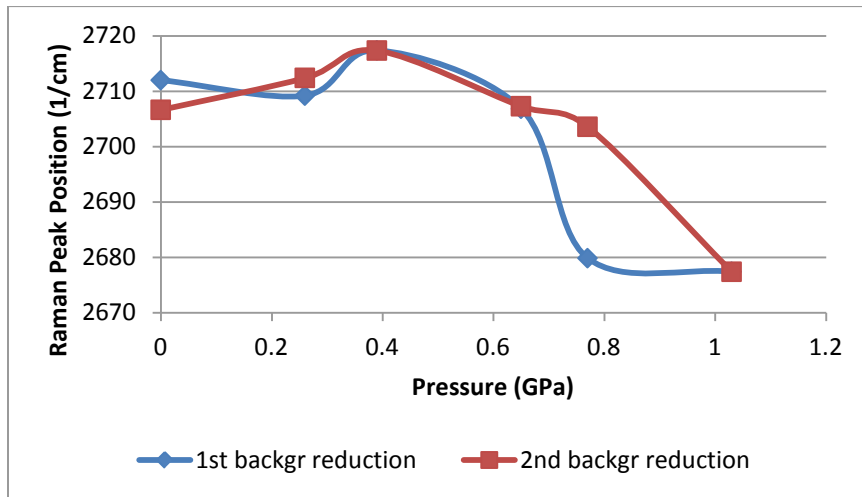


Figure 6-17

6.4.4. Partial pressure 150 mTorr

Low Range*

*partial pressure 150 and 175 were the only ones in which the D-peak could be observed

First background reduction (D-Peak)

Pressure	Ruby peak position	Number of peaks used to fit	peak position	FWHM	HWHM
0	694.64	12	1343.92	114.728	57.36
0.13	694.77	9	1348.78	155.213	77.607
0.26	694.9	14	1356.94	75.63	37.82
0.39	695.03	23	1335.31	113.701	56.85
0.52	695.16	22	1355.39	96.52	48.26
0.77	695.41	17	1363.92	94.65	47.32

Table 6-11

Second background reduction (D-Peak)

pressure	Ruby peak position	Number of peaks used to fit	peak position	FWHM	HWHM
0	694.64	12	1346.31	44.43	22.21
0.13	694.77	9	1343.5	41.181	20.59
0.26	694.9	17	1384	65.52	32.76
0.39	695.03	9	1342.87	62.67	31.34
0.52	695.16	19	1386	73.39	36.7
0.77	695.41	22	1387.5	65.313	-32.66

Table 6-12

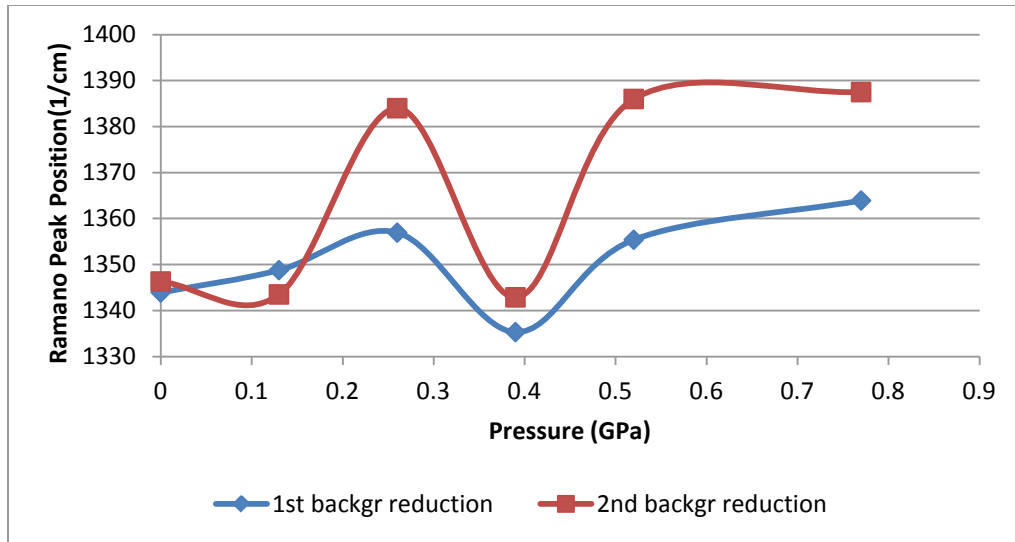


Figure 6-18

First background reduction (G-Peak)

pressure	Ruby peak position	Number of peaks used to fit	peak position	FWHM	HWHM
0	694.64	6	1619.55	171.249	85.62
0.13	694.77	9	1652.12	163.093	81.54626
0.26	694.9	14	1641.56	194.76	97.38
0.39	695.03	23	1613.45	128.864	-64.43
0.52	695.16	22	1600.41	169.198	84.6
0.77	695.41	17	1605.26	262.819	131.41

Table 6-13

Second background reduction (G-Peak)

pressure	Ruby peak position	Number of peaks used to fit	peak position	FWHM	HWHM
0	694.64	6	1619.55	171.249	85.62
0.13	694.77	9	1634.15	128.23	64.114
0.26	694.9	17	1630.28	96	48
0.39	695.03	9	1629.04	106.939	53.47
0.52	695.16	19	1609.85	105.57	52.78
0.77	695.41	22	1594.23	116.437	-58.22

Table 6-14

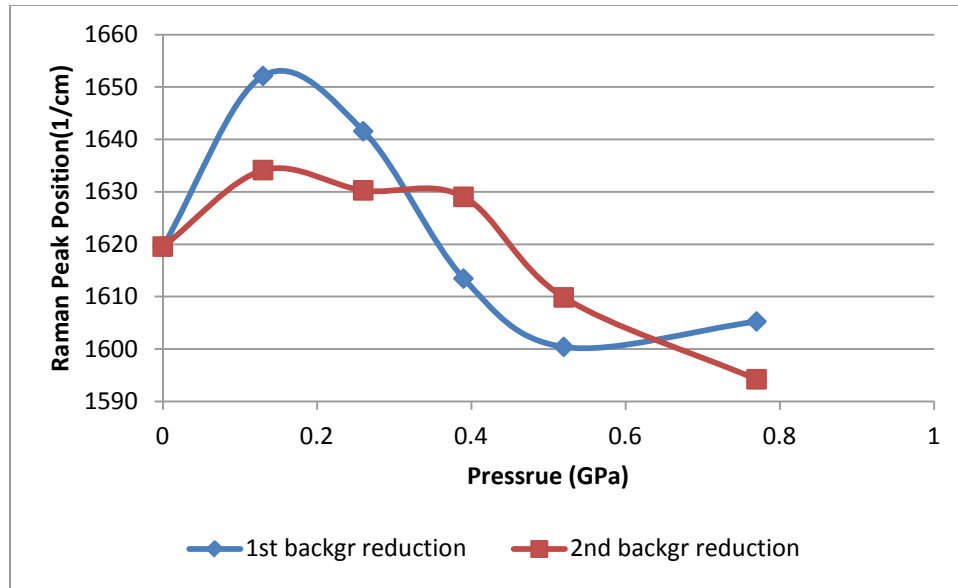


Figure 6-19

High range

pressure	Ruby peak position	Number of peaks used to fit	peak position	FWHM	HWHM
0	694.64	14	2701.37	83.34	41.69
0.13	694.77	7	2709.77	95.22	47.61
0.26	694.9	7(2 large peaks eliminated)	2702.79	203.942	101.97
0.39	695.03	6(2 large peaks eliminated)	2721.48	108.33	54.17
0.52	695.16	7(2 large peaks eliminated)	2676.99	200.34	100.17
0.77	695.41	5(2 large peaks eliminated)	2690.88	0.39	-0.195

Table 6-15

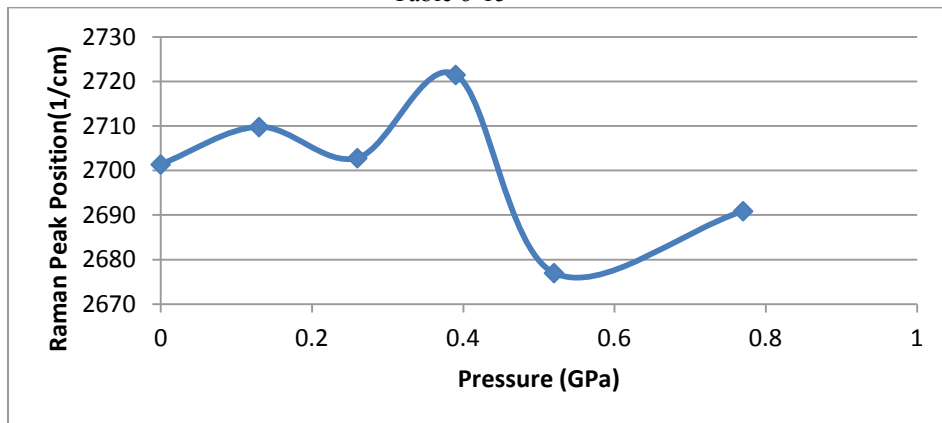


Figure 6-20

6.4.5. Partial pressure 175 mTorr

Low Range*

*partial pressure 150 and 175 were the only ones in which the D-peak could be observed

First background reduction (D-Peak)

pressure	Ruby peak position	Number of peaks used to fit	peak position	FWHM	HWHM
0.13	694.77	10	1313.67	153.855	76.93
0.26	694.9	18	1348.9	123.227	61.61
0.39	695.03	16	1338.2	130.94	65.47
0.65	695.29	14	1364.66	99.93	49.96
0.9	695.54	23	1339.88	86.97	43.48
1.29	695.93	17	1333.69	83.67	41.84

Table 6-16

Second background reduction (D-Peak)

pressure	Ruby peak position	Number of peaks used to fit	peak position	FWHM	HWHM
0.13	694.77	10	1324.26	53.87	-26.94
0.26	694.9	17	1352.98	53.79	26.89
0.39	695.03	16	1347.61	74.93	37.47
0.65	695.29	14	1389.36	69.74	34.87
0.9	695.54	12	1349.17	78.05	39.02
1.29	695.93	17	1345.45	73.79	36.89

Table 6-17

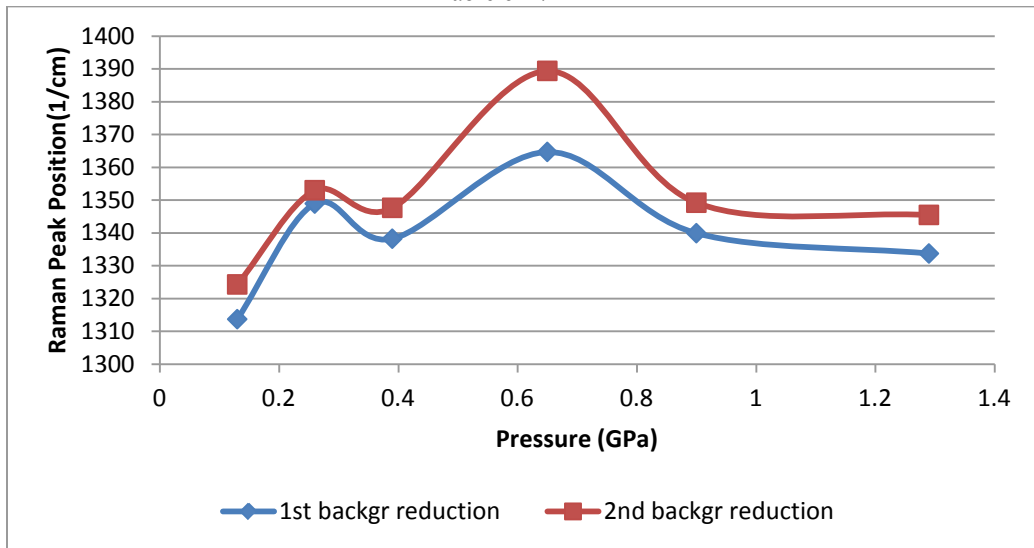


Figure 6-21

First background reduction (G-Peak)

pressure	Ruby peak position	Number of peaks used to fit	peak position	FWHM	HWHM
0.13	694.77	10	1609.57	110.05	55.023
0.26	694.9	18	1619.16	108.253	54.13
0.39	695.03	16	1647.6	163.94	81.6
0.65	695.29	14	1666.18	180.22	90.11
0.9	695.54	23	1663.84	164.74	83.37
1.29	695.93	17	1668.17	177.34	88.67

Table 6-18
Second background reduction (G-Peak)

pressure	Ruby peak position	Number of peaks used to fit	peak position	FWHM	HWHM
0.13	694.77	10	1628.09	111.85	55.92
0.26	694.9	17	1634.49	123.726	61.86
0.39	695.03	16	1656.69	105.279	52.64
0.65	695.29	14	1679.08	103.56	51.78
0.9	695.54	12	1669.95	101.445	50.72
1.29	695.93	17	1667.34	114.746	57.37

Table 6-19

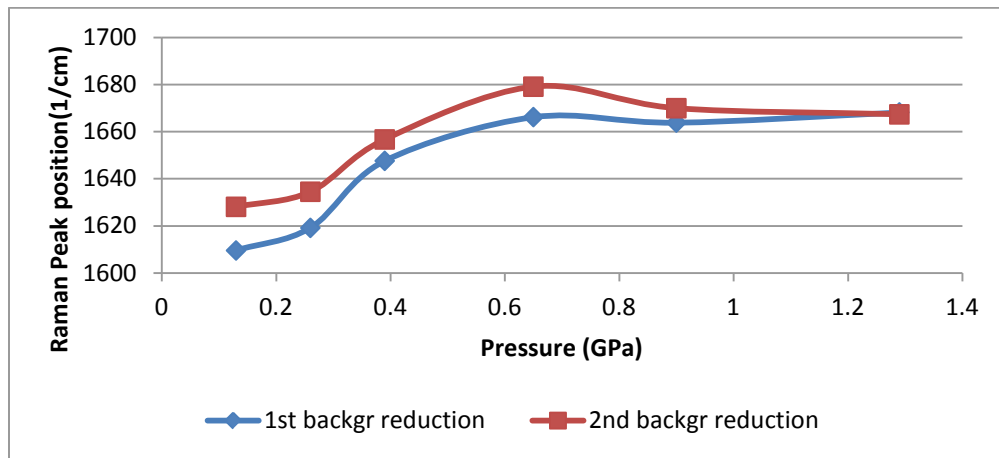


Figure 6-22

High range

pressure	Ruby peak position	Number of peaks used to fit	peak position	FWHM	HWHM
0.13	694.77	5	2640.31	467.13	233.565
0.26	694.9	5	2664.17	531.257	265.63
0.65	695.29	4	2578.85	94.96	47.48
0.9	695.54	3	2582.24	140.73	70.36
1.29	695.93	3	2578.22	94.88	47.44

Table 6-20

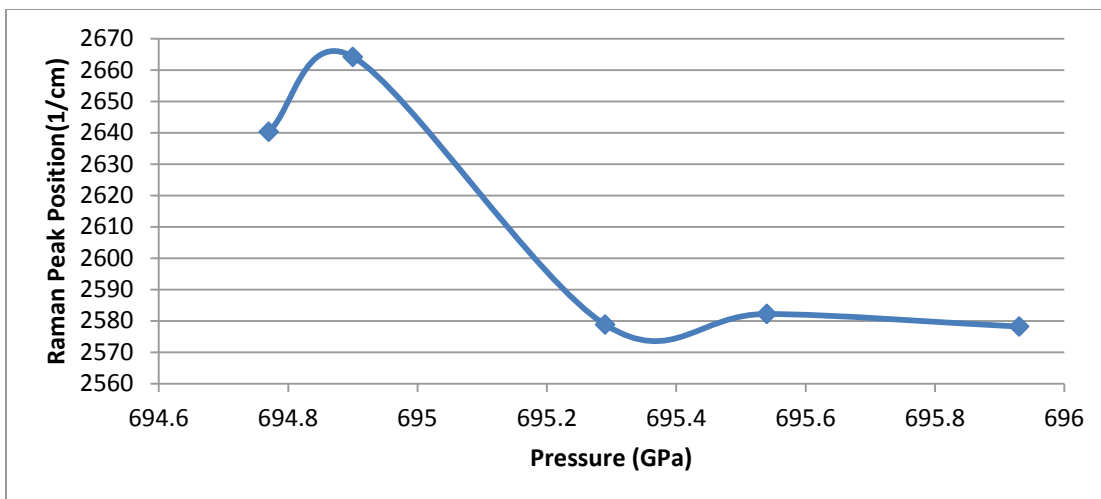


Figure 6- 23

6.5. Discussion and Conclusion

G peak positions and 2D peak positions are plotted versus pressure for the plasma treated samples (Figure 6-24). The data acquired using the diamond anvils are in good agreement with the previous studies on graphene under high pressure. Our experiments extended the pressure range up to 10 GPa, much higher than the pressure range of the previous data produced by Proctor et al.(2009).

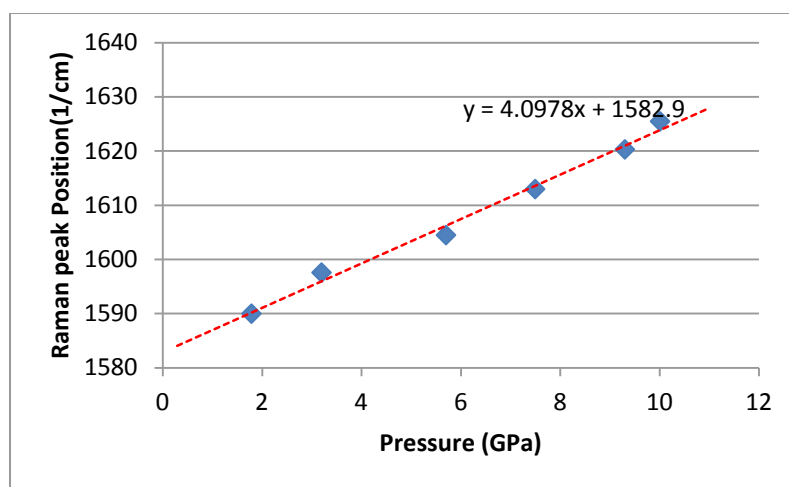


Figure 6-24
G-peak position vs pressure

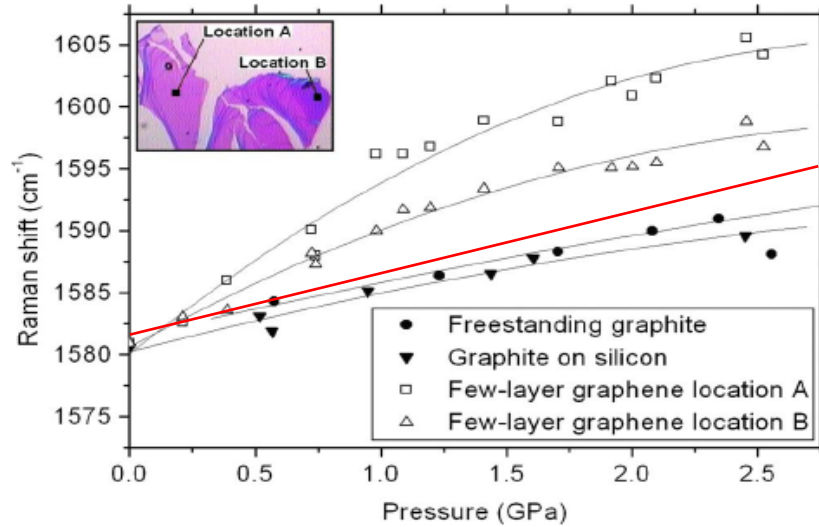


Figure 6-25

G-peak position in the Raman spectrum of graphene vs pressure. Red line plotted using the data collected in the current research, compared to data presented in other studies.^[5]

The points gathered using zirconia anvils seem to be scattered. The pressure limits reached using zirconia anvils are around 2GPa. The zirconia anvil produces high background in the Raman spectra. Also D peaks of graphene still cannot be observed although it was the main concern for using zirconia anvil cell instead of diamond anvil cell. Unlike what was expected diamond anvil cell seems to yield better results as compared to zirconia anvil cell. The only drawback for using diamonds is the fact that diamond has a sharp peak at ~ 1330 which overlaps the D peak of the graphene. Since while studying the Raman spectrum of the plasma treated graphene position of the D peak, its Shape and intensity are of critical importance, there will be a need to find a substitute for the diamond. The cubic zirconia seemed to be a proper candidate but throughout this research it was proven that the background is too high. For the aforementioned reason the D peak can not be studied on the spectrum recorded in a

zirconia loaded anvil either. When studying the plasma treated samples there are a number of parameters acting at the same time. This might explain getting the scattered data points. Based on the surface shape of the copper foil there might be different number of layers growing on the surface. This might be partially corrected by lapping the punched copper foils and making them as even as possible. This procedure should be done before the growth. Another point which might affect the results is that plasma treatment is basically making defects on the surface. There is no way to make sure that the defects on the surface are uniform and homogeneous. Also some oxygen atoms might be absorbed on the surface and absorption is not going to be homogeneous either. That implies that, there might be different number of layers and different thicknesses on one sample so for getting reasonable results on the effect of pressure on the sample laser beam should be always pointing to the exact same point. On the other hand laser beam can not be directed to the exact same point because when the pressure is increased the shape of the sample changes. All the above mentioned parameters might affect the position of the peak. So in order to have a precise explanation, the effects of multi layers of graphene, laser beam position, and plasma treatment should be taken into account and controlled. In conclusion from the data gathered in this research the slope of the pressure dependence of the G-band peak position reduces when graphene is plasma treated, and becomes negative when the partial pressure reaches 150 mTorr (with the exception of 75mTorr, which might be due to the experimental error). Raman G peak shift slope is decreasing as the pressure is increased a trend which has been observed in other publications as well.^[5] The FWHM shows a considerable broadening for 2D peak after plasma treatment which also has been observed by Nourbakhsh et al. (2010).

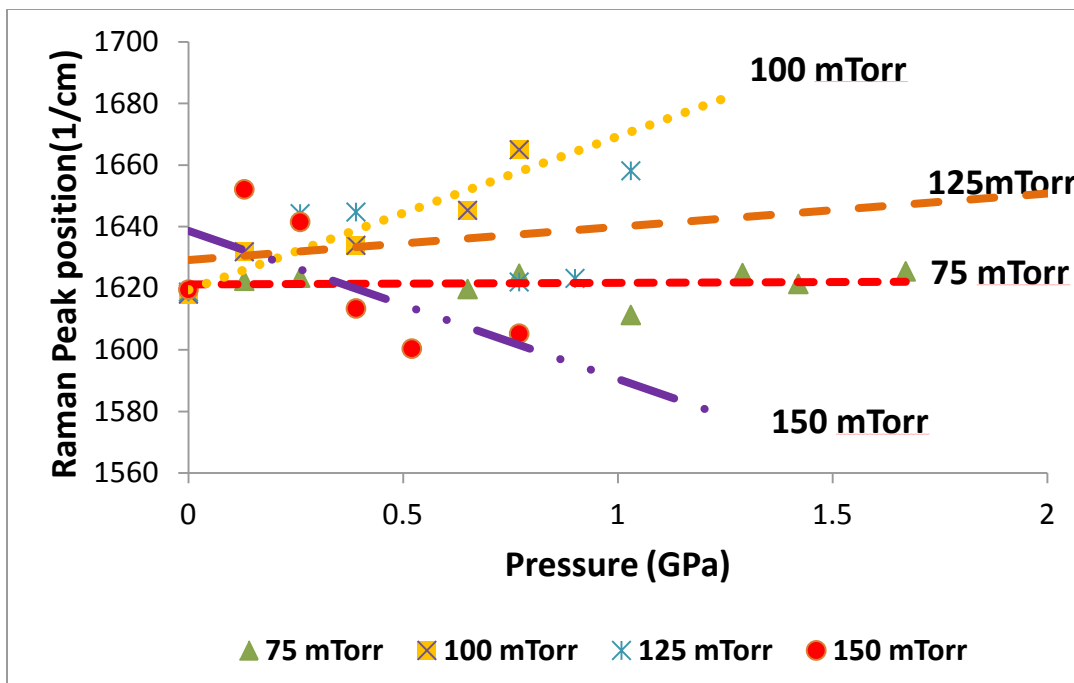


Figure 6-26
G-peak position vs Pressure points collected by Zr anvils

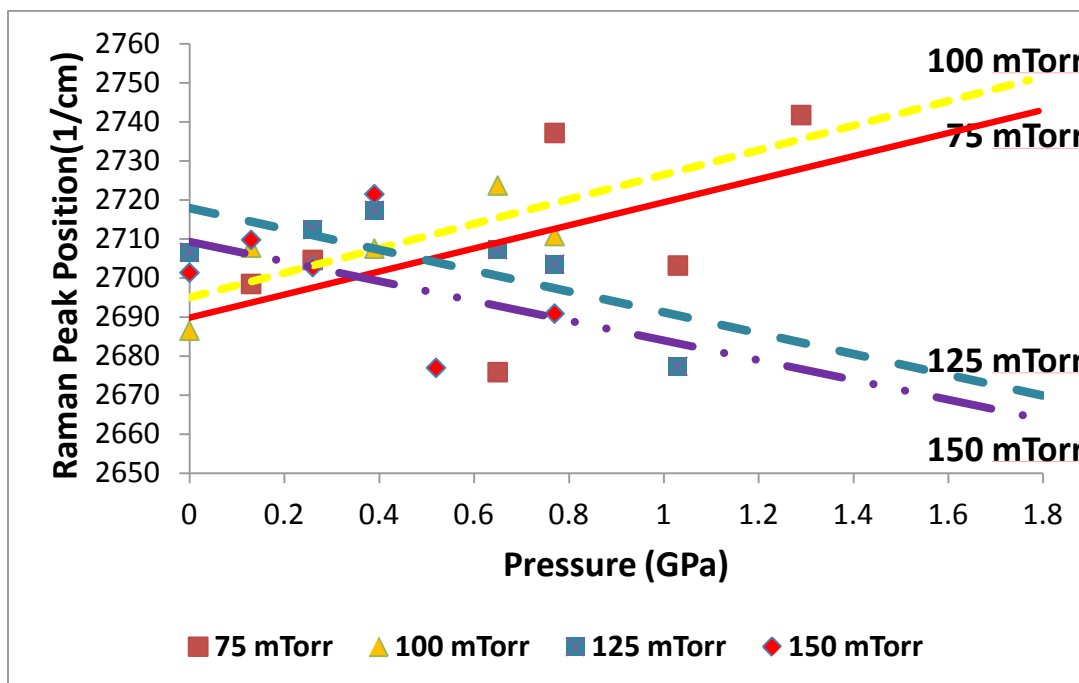


Figure 6-27
2D-peak position vs Pressure points collected by Zr anvils

6.6. Future work

Due to the scattered nature of the results it is hard to judge on them. There is not a single trend by which observations can be explained and the results can be justified. But by referring to the literature there are already articles published on Raman spectroscopy of graphene under high pressure. Although, at the time of writing this research there was no published article on Raman spectroscopy of plasma treated graphene it could be assumed Raman spectroscopy of plasma treated graphene should yield the similar results as the Raman spectroscopy of nontreated one.^[5] If so still the scattered nature of the Raman shift of each set of plasma treated graphene with increasing pressure and not being able to see the the D-peaks in some the samples as compared to other ones stays unexplained. Even assuming that not being able to see the D-peak is a result of experimental error which occurred due to laser beam aiming at a point which does have the graphene coat on, does not resolve much. If so all the results except for the partial pressures 150 mTorr and 175 mTorr should be disregard. But even that will not solve the inconsistency of the results. To make sure about the accuracy of the results another set of experiments with CZ should be performed but due to the nature of CZ and being unable to further increase the pressure. The same set could be done using Moissanite anvils. Using which there is no need to change the anvils after each run, increasing the pressure in the range needed is not a problem and last but not the least Moissanite peaks will not overlap that of the graphene.

LIST OF REFERENCES

- [1]. A. Geim (2009), Science 324:5934, 1530-1534 (2009)
- [2]. A. C. Ferrari, J.C. Meyer (2006), Phys. Rev. Lett. 97, 187401(2006)
- [3]. L.M. Malarda M.A. Pimenta (2009), PHYSICS REPORTS 473, 5187(2009)
- [4]. A. Nourbakhsh, Mirco Cantoro (2010), Nanotechnology 21, 435203(2010)
- [5]. John E. Proctor, Eugene Gregoryanz (2009), Phys. Rev. B 80, 073408 (2009)
- [6]. J. C. Meyer, A. Geim (2007), Nature LETTERS, 446, 60-63, 10-1038
- [7]. D. A. Long, "Raman Spectroscopy", McGraw-Hill Inc, 1977, ISBN 0-07-038675-7
- [8]. Changgu Lee (2008), Science 321-385 (2008)
- [9]. Nicolas Moral, "Production and Characterization of Carbon-based Materials", Lulea University of Technology ISSN 1653-0187
- [10]. Jae Eun Oh, Simon M. Clark (2012) Cement and Concrete Research, 42,397-403
- [11]. A. JayaRaman (1983) RevModPhys.55.65
- [12]. N. R. Jackson (2010), Review of Scientific Instruments 81-073902 (2010)
- [13]. Ved Prakash Verma, Santanu Das (2010), APPLIED PHYSICS LETTERS 96, 203108 (2010)
- [14]. F. Schedin, A. K. Geim (2007), Nature Materials 6, 652-655 (2007)
- [15]. Zhongqing Wei, Debin Wang (2010), Science 328, 1373 (2010)
- [16]. W. A. Bassett, High Pressure Research(2009), 29:2,163-186 (2009)
- [17]. D. J. Dunstan (1989), J. Phys. E:sci. Instrum 22, 913-923 (1989)
- [18]. J. Xu and E. Huang, Rev. Sci. Instrum. 65, 204 (1994)
- [19]. D. E. Patterson and J. L. Margrave, J. Phys. Chem. 94, 1094 (1990)
- [20]. Wongbong Choi, I. Lahiri, Critical Reviews in Solid State and Materials Sciences, 35:1, 52-71 (2010)
- [21]. Ji-an Xu, Ho-Kwang Mao, J. Phys. Condens. Matter 14 11543 (2002)

[22]. Ji-an Xu, Ho-Kwang Mao, Science 290, 783 (2000)